Herzog C, Sales N, Etchegaray N, Charbonnier A, Freire S, Dormont D, Deslys JP, Lasmezas CI (2004) Tissue distribution of bovine spongiform encephalopathy agent in primates after intravenous or oral infection. Lancet 363:422–428

Hill AF, Butterworth RJ, Joiner S, Jackson G, Rossor MN, Thomas DJ, Frosh A, Tolley N, Bell JE, Spencer M, King A, Al-Sarraj S, Ironside JW, Lantos PL, Collinge J (1997) Diagnosis of new variant Creutzfeldt-Jakob disease by tonsil biopsy. Lancet 349:99–100

Hill AF, Butterworth RJ, Joiner S, Jackson G, Rossor MN, Thomas DJ, Frosh A, Tolley N, Bell JE, Spencer M, King A, Al-Sarraj S, Ironside JW, Lantos PL, Collinge J (1999) Investigation of variant Creutzfeldt-Jakob disease and other human prion diseases with tonsil biopsy samples. Lancet 353:183–189

Horiuchi M, Yamazaki N, Ikeda T, Ishiguro N, Shinagawa M (1995) A cellular form of prion protein (PrP^{C}) exists in many non-neuronal tissues of sheep. J Gen Virol 76:2583–2587

Huang FP, Farquhar CF, Mabbott NA, Bruce ME, MacPherson GG (2002) Migrating intestinal dendritic cells transport PrP(Sc) from the gut. J Gen Virol 83:267–271

Iwanaga T, Han H, Hoshi O, Kanazawa H, Adachi I, Fujita T (1994) Topographical relation between serotonin-containing paraneurons and peptidergic neurons in the intestine and urethra. Biol Signals 3(5):259–270

Jenny M, Uhl C, Roche C, Duluc I, Guillermin V, Guillemot F, Jensen J, Kedinger M, Gradwohl G (2002) Neurogenin3 is differentially required for endocrine cell fate specification in the intestinal and gastric epithelium. EMBO J 21:6338–6347

Kitamoto T, Muramoto T, Mohri S, Doh-Ura K, Tateishi J (1991) Abnormal isoform of prion protein accumulates in follicular dendritic cells in mice with Creutzfeldt-Jakob disease. J Virol 65:6292–6295

Mabbott NA, Williams A, Farquhar CF, Pasparakis M, Kollias G, Bruce ME (2000) Tumor necrosis factor alpha-deficient, but not interleukin-6-deficient, mice resist peripheral infection with scrapie. J Virol 74:3338–3344

Mabbott NA, Young J, McConnell I, Bruce ME (2003) Follicular dendritic cell dedifferentiation by treatment with an inhibitor of the lymphotoxin pathway dramatically reduces scrapie susceptibility. J Virol 77:6845–6854

Manson JC, Clarke AR, McBride PA, McConnell I, Hope J (1994) PrP gene dosage determines the timing but not the final intensity or distribution of lesions in scrapie pathology. Neurodegeneration 3:331–340

Marcos Z, Pffeifer K, Bodegas ME, Sesma MP, Guembe L (2004) Cellular prion protein is expressed in a subset of neuroendocrine cells of the rat gastrointestinal tract. J Histochem Cytochem 52:1357–1365

Marcos Z, Bodegas ME, Sesma MP, Guembe L (2005a) Characterization of PrPc-immunoreactive cells in monkey (Macaca fascicularis) gastrointestinal tract. Ann N Y Acad Sci 1040:387–390

Marcos Z, Bodegas ME, Sesma MP, Guembe L (2005b) Comparative Study of PrPc Expression in Rat, Monkey, and Cow Gastrointestinal Tract. Ann N Y Acad Sci 1040:391–394

Marsh RF, Bessen RA, Lehmann S, Hartsough GR (1991) Epidemiological and experimental studies on a new incident of transmissible mink encephalopathy. J Gen Virol 72:589–594

McBride PA, Eikelenboom P, Kraal G, Fraser H, Bruce ME (2002) PrP protein is associated with follicular dendritic cells of spleens and lymph nodes in uninfected and scrapie-infected mice. J Pathol 168:413–418

Miyazawa K, Aso H, Kanaya T, Kido T, Minashima T, Watanabe K, Ohwada S, Kitazawa H, Rose MT, Tahara K, Yamasaki T, Yamaguchi T (2006a) Apoptotic process of porcine intestinal M cells. Cell Tissue Res 323:425–432

Miyazawa K, Aso H, Honda M, Kido T, Minashima T, Kanaya T, Watanabe K, Ohwada S, Rose MT, Yamaguchi T (2006b) Identification of bovine dendritic cell phenotype from bovine peripheral blood. Res Vet Sci 81:40–45

Montrasio F, Frigg R, Glatzel M, Klein MA, Mackay F, Aguzzi A, Weissmann C (2000) Impaired prion replication in spleens of mice lacking functional follicular dendritic cells. Science 288:1257–1259

Nakamura F, Seki I, Kobayashi K, Tanaka M, Fukunaga S (2002) Immunohistochemical detection of cellular prion protein (PrPc) in the rat central nervous system. Animal Sci J 73:553–556

Prinz M, Huber G, Macpherson AJ, Heppner FL, Glatzel M, Eugster HP, Wagner N, Aguzzi A (2003) Oral prion infection requires normal numbers of Peyer's patches but not of enteric lymphocytes. Am J Pathol 162:1103–1111

Prusiner SB(1982) Novel proteinaceous infectious particles cause scrapie. Science 216:136–144

Prusiner SB (1998) Prions. Proc Natl Acad Sci USA 95:13363–13383

Race R, Oldstone M, Chesebro B (2000) Entry versus blockade of brain infection following oral or intraperitoneal scrapie administration: role of prion protein expression in peripheral nerves and spleen. J Virol 74:828–833

Rescigno M, Urbano M, Valzasina B, Francolini M, Rotta G, Bonasio R, Granucci F, Kraehenbuhl JP, Ricciardi-Castagnoli P (2001) Dendritic cells express tight junction proteins and penetrate gut epithelial monolayers to sample bacteria. Nat Immunol 2:361–367

Sakaguchi S, Katamine S, Nishida N, Moriuchi R, Shigematsu K, Sugimoto T, Nakatani A, Kataoka Y, Houtani T, Shirabe S, Okada H, Hasegawa S, Miyamoto T, Noda T (1996) Loss of cerebellar Purkinje cells in aged mice homozygous for a disrupted PrP gene. Nature 380:528–531

Schreuder BE, van Keulen LJ, Vromans ME, Langeveld JP, Smits MA (1998) Tonsillar biopsy and PrPSc detection in the preclinical diagnosis of scrapie. Vet Rec 142:564–568

Shlomchik MJ, Radebold K, Duclos N, Manuelidis L (2001) Neuroinvasion by a Creutzfeldt-Jakob disease agent in the absence of B cells and follicular dendritic cells. Proc Natl Acad Sci USA 98:9289–9294

Sigurdson CJ, Barillas-Mury C, Miller MW, Oesch B, van Keulen LJ, Langeveld JP, Hoover EA (2002) PrP(CWD) lymphoid cell targets in early and advanced chronic wasting disease of mule deer. J Gen Virol 83:2617–2628

Somerville RA, Birkett CR, Farquhar CF, Hunter N, Goldmann W, Dornan J, Grover D, Hennion RM, Percy C, Foster J, Jeffrey M (1997) Immunodetection of PrPSc in spleens of some scrapie-infected sheep but not BSE-infected cows. J Gen Virol 78:2389–2396

Sugaya M, Nakamura K, Watanabe T, Asahina A, Yasaka N, Koyama Y, Kusubata M, Ushiki Y, Kimura K, Morooka A, Irie S, Yokoyama T, Inoue K, Itohara S, Tamaki K (2002) Expression of cellular prion-related protein by murine Langerhans cells and keratinocytes. J Dermatol Sci 28:126–134

Terry LA, Marsh S, Ryder SJ, Hawkins SA, Wells GA, Spencer YI (2003) Detection of disease-specific PrP in the distal ileum of cattle exposed orally to the agent of bovine spongiform encephalopathy. Vet Rec 152:387–392

Thielen C, Melot F, Jolois O, Leclercq F, Tsunoda R, Frobert Y, Heinen E, Antoine N (2001a) Isolation of bovine follicular dendritic cells allows the demonstration of a particular cellular prion protein. Cell Tissue Res 306:49–55

Thielen C, Antoine N, Melot F, Cesbron JY, Heinen E, Tsunoda R (2001b) Human FDC express PrPc in vivo and in vitro. Dev Immunol 8:259–266

van Keulen LJ, Schreuder BE, Meloen RH, Mooij-Harkes G, Vromans ME, Langeveld JP (1996) Immunohistochemical detection of prion protein in lymphoid tissues of sheep with natural scrapie. J Clin Microbiol 34:1228–1231

Wadsworth JD, Joiner S, Hill AF, Campbell TA, Desbruslais M, Luthert PJ, Collinge J (2001) Tissue distribution of protease resistant prion protein in variant Creutzfeldt-Jakob disease using a highly sensitive immunoblotting assay. Lancet 358:171–80

Wells GA, Dawson M, Hawkins SA, Green RB, Dexter I, Francis ME, Simmons MM, Austin AR, Horigan MW (1994) Infectivity in the ileum of cattle challenged orally with bovine spongiform encephalopathy. Vet Rec 135:40–41

Will RG, Ironside JW, Zeidler M, Cousens SN, Estibeiro K, Alperovitch A, Poser S, Pocchiari M, Hofman A, Smith PG (1996) A new variant of Creutzfeldt-Jakob disease in the UK. Lancet 347:921–925

Available online at www.sciencedirect.com
ScienceDirect
ELSEVIER
Gene 386 (2007) 139–146
GENE
SECTION
FUNCTIONAL GENOMICS
www.elsevier.com/locate/gene

Newly established *in vitro* system with fluorescent proteins shows that abnormal expression of downstream prion protein-like protein in mice is probably due to functional disconnection between splicing and 3′ formation of prion protein pre-mRNA

Daisuke Yoshikawa [a], Juraj Kopacek [a,b], Naohiro Yamaguchi [a], Daisuke Ishibashi [c], Hitoki Yamanaka [c], Yoshitaka Yamaguchi [c], Shigeru Katamine [a], Suehiro Sakaguchi [a,c,d,*]

[a] *Department of Molecular Microbiology and Immunology, Nagasaki University Graduate School of Biomedical Sciences, Sakamoto 1-12-4, Nagasaki 852-8523, Japan*
[b] *Department of Molecular Biology, Institute of Virology, Slovak Academy of Sciences, Bratislava, Slovakia*
[c] *PRESTO Japan Science and Technology Agency, 4-1-8 Honcho Kawaguchi, Saitama, Japan*
[d] *Division of Molecular Cytology, Institute for Enzyme Research, The University of Tokushima, 3-18-15 Kuramoto-cho, Tokushima 770-8503, Japan*

Received 10 July 2006; received in revised form 8 August 2006; accepted 25 August 2006
Available online 15 September 2006
Received by A. Bernardi

Abstract

We and others previously showed that, in some lines of prion protein (PrP)-knockout mice, the downstream PrP-like protein (PrPLP/Dpl) was abnormally expressed in brains partly due to impaired cleavage/polyadenylation of the residual PrP promoter-driven pre-mRNA despite the presence of a poly(A) signal. In this study, we newly established an *in vitro* transient transfection system in which abnormal expression of PrPLP/Dpl can be visualized by expression of the green fluorescence protein, EGFP, in cultured cells. No EGFP was detected in cells transfected by a vector carrying a PrP genomic fragment including the region targeted in the knockout mice intact upstream of the PrPLP/Dpl gene. In contrast, deletion of the targeted region from the vector caused expression of EGFP. By employing this system with other vectors carrying various deletions or point mutations in the targeted region, we identified that disruption of the splicing elements in the PrP terminal intron caused the expression of EGFP. Recent lines of evidence indicate that terminal intron splicing and cleavage/polyadenylation of pre-mRNA are functionally linked to each other. Taken together, our newly established system shows that the abnormal expression of PrPLP/Dpl in PrP-knockout mice caused by the impaired cleavage/polyadenylation of the PrP promoter-driven pre-mRNA is due to the functional dissociation between the pre-mRNA machineries, in particular those of cleavage/polyadenylation and splicing. Our newly established *in vitro* system, in which the functional dissociation between the pre-mRNA machineries can be visualized by EGFP green fluorescence, may be useful for studies of the functional connection of pre-mRNA machineries.

Keywords: Intergenic splicing; *In vitro* system; Purkinje cell degeneration; Fluorescent protein

1. Introduction

Prnd is a recently identified gene encoding the first prion protein (PrP)-like protein, PrPLP/Doppel (Dpl), locating 16-kb downstream of the PrP gene, *Prnp* (Moore et al., 1999; Li et al., 2000a). *Prnd* is actively expressed in the testis, heart, skeletal muscle, and spleen, but not in the brain, whereas *Prnp* is the most abundantly expressed in the brain (Li et al., 2000b). Male mice devoid of PrPLP/Dpl were shown to be infertile due to

Abbreviations: PrP, prion protein; PrPLP/Dpl, PrP-like protein/Doppel; bp, base pair; PCR, polymerase chain reaction; nt, nucleotides; EGFP, enhanced green fluorescence protein; UTR, untranslated region; ORF, open reading frame; DMEM, Dulbecco's Modified Eagle Medium; RACE, rapid amplification of cDNA ends; HCMV, human cytomegalovirus; RNP, ribonucleoprotein; PAP, poly(A) polymerase; CPSF, cleavage/polyadenylation specificity factor.

* Corresponding author. Division of Molecular Cytology, Institute for Enzyme Research, The University of Tokushima, 3-18-15 Kuramoto-cho, Tokushima 770-8503, Japan. Tel.: +81 88 633 7438; fax: +81 88 633 7440.
E-mail address: sakaguch@ier.tokushima-u.ac.jp (S. Sakaguchi).

0378-1119/$ - see front matter © 2006 Elsevier B.V. All rights reserved.
doi:10.1016/j.gene.2006.08.028

abnormal development of sperm, indicating that PrPLP/Dpl is important for spermatogenesis (Behrens et al., 2002).

We and others found that PrPLP/Dpl is toxic when ectopically expressed in neurons deficient for the cellular PrP (PrP^C) (Moore et al., 2001; Anderson et al., 2004; Yamaguchi et al., 2004). Some lines of mice devoid of PrP^C ($Prnp^{0/0}$), including Ngsk $Prnp^{0/0}$, Rcm0 $Prnp^{0/0}$, and Zrch II $Prnp^{0/0}$, developed ataxia and Purkinje cell degeneration due to the ectopic expression of PrPLP/Dpl in neurons, but others, such as Zrch I $Prnp^{0/0}$ and Npu $Prnp^{0/0}$, showed neither the ectopic expression of PrPLP/Dpl nor such neurological abnormalities (Bueler et al., 1992; Manson et al., 1994; Sakaguchi et al., 1996; Moore et al., 1999; Rossi et al., 2001). In the ataxic lines of $Prnp^{0/0}$ mice, *Prnd* was aberrantly regulated under the control of *Prnp* promoter and thereby ectopically expressed in the brain, especially in neurons, where the *Prnp* promoter is very active (Moore et al., 1999; Li et al., 2000a). The ectopically expressing PrPLP/Dpl mRNAs were chimeric, comprising the residual *Prnp* non-coding exons 1 and 2 at the 5′ end followed by the *Prnd*-coding exons, due to an abnormal intergenic splicing taking place between *Prnp* and *Prnd* (Moore et al., 1999; Li et al., 2000a). The mechanism of how *Prnd* became abnormally regulated under the control of the *Prnp* promoter in the ataxic lines of $Prnp^{0/0}$ mice remains to be studied.

In wild-type mice, PrP pre-mRNA is normally cleaved and polyadenylated at the end of *Prnp*. However, in ataxic lines of $Prnp^{0/0}$ mice, the pre-mRNA was unsuccessfully cleaved and polyadenylated at the end of *Prnp*, resulting in its elongation until the end of downstream *Prnd* (Moore et al., 1999; Li et al., 2000a), indicating that the abnormal regulation of *Prnd* in these mice could be in part attributable to the impaired cleavage/polyadenylation of *Prnp* pre-mRNA. A polyadenylation signal is essential for the pre-mRNA cleavage/polyadenylation processes. However, the polyadenylation signal of *Prnp* and its flanking sequences are intact in two ataxic lines of Ngsk $Prnp^{0/0}$ and Rcm0 $Prnp^{0/0}$ mice. It is recently believed that the pre-mRNA processes, including acquisition of a cap structure at the 5′ end, splicing out of introns, and cleavage/polyadenylation at the 3′ end, are functionally linked to each other during transcription (Steinmetz, 1997; Proudfoot et al., 2002; Kornblihtt et al., 2004). In particular, the cleavage/polyadenylation processes are strongly influenced by splicing of the terminal intron. In the ataxic lines of $Prnp^{0/0}$ mice, a part of the *Prnp* terminal intron including the elements important for splicing, such as a splice branch point, a polypyrimidine tract, and a splice acceptor, is commonly targeted as well as the subsequent half of the last exon (Sakaguchi et al., 1995; Moore et al., 1999; Rossi et al., 2001). Thus, disruption of these splicing elements due to deletion of intron 2 could cause functional dissociation between splicing and cleavage/polyadenylation for the *Prnp* pre-mRNA in the ataxic lines of $Prnp^{0/0}$ mice, resulting in the impaired cleavage/polyadenylation of the pre-mRNA. It is alternatively possible that deletion of the exonic sequences in *Prnp* might disturb the cleavage/polyadenylation processes for the *Prnp* pre-mRNA.

In the present study, we established an *in vitro* transient transfection system in which abnormal expression of PrPLP/Dpl can be visualized by expression of the green fluorescence protein, EGFP, in cultured cells. Using this system, we identified that the abnormal expression of PrPLP/Dpl could be attributed to the functional disconnection between splicing and cleavage/polyadenylation processes. These results indicate usefulness of our newly established *in vitro* system for studying the functional connection of pre-mRNA machineries because the functional dissociation between the pre-mRNA machineries can be easily visualized by EGFP green fluorescence.

2. Materials and methods

2.1. Expression vectors

2.1.1. pPrPwild

The 488- and 2688-bp genomic fragments of *Prnd*, spanning nucleotides (nt) 35,716 to 36,204 (GenBank accession no. *U29187*) and nt 36,712 to 39,400, respectively, were first amplified from mouse genomic DNA using polymerase chain reaction (PCR; Advantage cDNA PCR KIT, Clontech, California, USA) with appropriate sets of a primer pair. The former, corresponding to a part of intron 1 and an entire 5′ untranslated region (UTR) of *Prnd*, possessed the *Sal* I and *Nhe* I enzyme sites at the 5′ and 3′ ends, respectively. The latter, consisting of an entire 3′ UTR and the downstream intervening sequence, had the *Bam*H I and *Mlu* I sites at its 5′ and 3′ ends, respectively. These fragments were ligated with the enhanced green fluorescence protein (EGFP)-coding *Nhe* I–*Bam*H I insert of pEGFP-C1 (Clontech) in such a way that the EGFP insert was flanked by the genomic fragments, and cloned into the *Sal* I and *Mlu* I sites of a pDON-AI plasmid (Takara, Tokyo, Japan) with a newly created *Mlu* I site at the multiple cloning site, yielding the plasmid pPrnd-EGFP. Next, two *Prnp* genomic DNAs, the 806-bp fragment from nt 18,861 to 19,667 encompassing a part of intron 2 and an entire 5′ UTR of exon 3 and the 1699-bp DNA from nt 20,442 to 22,140 consisting of an entire 3′ UTR and the downstream intervening sequence, were amplified by PCR. The former possessed the artificial *Spe* I and *Bam*H I enzyme sites at the 5′ and 3′ ends, respectively, and the latter contained the *Not* I and *Sal* I sites at the 5′ and 3′ ends, respectively. These fragments were ligated with the DsRed-coding *Bam*H I–*Not* I insert of pDsRed1-N1 (Clontech) in such a way that the insert was flanked by the two genomic fragments, and cloned into the *Spe* I and *Sal* I sites of pPrnd-EGFP, resulting in pPrPwild.

2.1.2. pPrP5′targeted

The 750-bp (from nt 18,661 to 19,411) fragment of *Prnp* intron 2, containing *Spe* I and *BamH* I sites at the 5′ and 3′ ends, respectively, was generated by PCR with a primer pair, and then placed for the corresponding fragment in pPrPwild, resulting in pPrP5′targeted.

2.1.3. pPrPint2(-3), pPrPint2(-26), pPrPint2(-50)

The *Prnp* intron 2 containing either 3-bp from nt 19,664 to 19,666, 26-bp from nt 19,641 to 19,666, or 50-bp from nt 19,617 to 19,666, together with the 5′ UTR of exon 3 and the

DsRed open reading frame (ORF), was amplified by PCR with a primer pair using pPrPwild as a template. *Bgl* II and *Not* I sites were introduced at the 5′ and 3′ ends of each fragment, respectively. These amplified fragments were placed for the corresponding fragment in pPrP5′targeted, respectively, yielding pPrPint2(-3), pPrPint2(-26) and pPrPint2(-50).

2.1.4. pPrP3′targeted and pPrPtargeted

A genomic fragment from nt 20,893 (corresponding to the *Eco*R I site in *Prnp* exon 3) to 22,140, encompassing a part of 3′ UTR and the downstream intervening sequence, was amplified by PCR using pPrPwild as a template with primers, each containing the *Not* I or *Sal* I recognition sequences. This amplified fragment was placed for the corresponding *Not* I–*Sal* I fragment in pPrPwild, producing a pPrP3′targeted plasmid. Moreover, pPrPtargeted was constructed by replacing this amplified fragment with the corresponding fragment in pPrP5′ targeted.

2.1.5. pPrPint2(-26)AG, pPrPint2(-26)Br, pPrPint2(-26)Br2×, pPrPint2(-26)AGBr2×

To construct these vectors, point mutations were introduced using a QuickChange Site-Directed Mutagenesis Kit (Stratagen, La Jolla, CA) using pPrPint2(-26) as a template. The mutations were verified by DNA sequencing.

2.2. Transfection and fluorescent microscopic analysis

Plasmids were transfected into mouse neuroblastoma N2a cells, which were maintained at 37 °C under 5% CO_2 in Dulbecco's Modified Eagle Medium (DMEM) supplemented with 10% fetal bovine serum. 2×10^5 cells were plated in one well of a 6-well plate and transfected by plasmids using Lipofectamin 2000 reagent (Invitrogen life technologies, Carlsbad, CA) the next day, as recommended by the manufacturer. Cells were inspected 48 h after transfection by fluorescence microscopy.

2.3. 3′ Rapid amplification of cDNA ends (RACE)

Total RNA was isolated from the cells 48 h after transfection using a Trizol reagent (Invitrogen life technologies). 1 μg of total RNA was subjected to first strand cDNA synthesis with Oligo dT-3 sites Adaptor Primer using the 3′-Full RACE Core Set (Takara) according to the manufacturer's recommendations. The synthesized cDNAs were subsequently amplified directly by PCR using the R-U5-3* primer, 5′-AGTGATTGACTACCC GTCAGCGGGGGTC-3′, and the 3 sites Adaptor Primer, 5′-CTGATCTAGAGGTACCGGATCC-3′.

2.4. DNA sequencing

DNA sequences were determined by the chain termination reaction method using Texas Red labeled specific primers (Amersham) and the ThermoSequenase premixed cycle sequencing kit (Amersham) according to the manufacturer's recommendations.

3. Results and discussion

3.1. Establishment of an in vitro transient transfection system to easily detect abnormal expression of PrPLP/Dpl by EGFP fluorescent protein

To establish an *in vitro* transient transfection system, in which the intergenic splicing-mediated abnormal expression of PrPLP/Dpl in ataxic lines of $Prnp^{0/0}$ mice can be mimicked in cultured cells, we first constructed two expression vectors, termed pPrPwild and pPrPtargeted. pPrPwild contained a part of *Prnp* genomic DNA including 816-bp of the 3′ part of intron 2, the entire exon 3, and the 3′ intervening sequence, followed by a *Prnd* genomic fragment comprising intron 1, exon 2, intron 2, exon 3 and the 3′ intervening sequence (Fig. 1B). In this vector, transcription is engineered to start from the upstream vector-derived exon under the control of the immediate early gene promoter of human cytomegalovirus (HCMV) and terminate at the end of *Prnp* exon 3 using its native poly(A) signal (Fig. 1B). We also replaced the *Prnp*- and *Prnd*-coding sequences with those of the fluorescent proteins, DsRed and EGFP, respectively (Fig. 1B), to easily detect expression of the *Prnp*- or the *Prnd*-coding exon under fluorescence microscopy. pPrPtargeted lacks the same *Prnp* region as in the ataxic lines of $Prnp^{0/0}$ mice, including 250-bp of intron 2, 10-bp of the 5′ UTR, the entire PrP ORF, and 450-bp of the 3′ UTR (Fig. 1A and B).

We then transfected these vectors into mouse N2a neuroblastoma cells and carried out a fluorescent microscopic examination 48 h after transfection. We also characterized the transcripts expressed from the vectors in these transfected cells by a 3′ RACE cloning technique and subsequent DNA sequencing. The pPrPwild-transfected cells produced DsRed fluorescence alone (Fig. 1C). No EGFP expression could be detected in these cells (Fig. 1C). 3′ RACE of the total RNA extracted from these transfected cells revealed several distinct bands, including one major and a few minor bands, on an agarose gel (Fig. 2A). We cloned the major band and determined its DNA sequence. The major transcript consisted of the vector-derived exon and *Prnp* exon 3 followed by a poly(A) tail (Fig. 2B), indicating that transcription was started from the vector-derived exon, terminating at the end of the *Prnp* exon 3, being subjected to splicing between these two exons. In contrast, pPrPtargeted produced only green EGFP but not DsRed fluorescence in the cells (Fig. 1C). 3′ RACE of these cells produced one major and a few minor bands on an agarose gel (Fig. 2A). DNA sequencing of the major band showed that it comprised the vector-derived exon and the downstream *Prnd* exons (Fig. 2B), indicating that the pre-mRNA started from the vector-derived exon was unsuccessfully terminated at the end of the *Prnp* terminal exon 3, elongated to the *Prnd* terminal exon 3, and subsequently underwent aberrant splicing between the vector-derived exon and the *Prnd* exons 2 and 3. This abnormal processing of the pre-mRNA expressed from pPrPtargeted in N2a cells is very similar to that for the targeted *Prnp* allele in the ataxic lines of $Prnp^{0/0}$ mice (Moore et al., 1999; Li et al., 2000a), whereas the processing for the pre-mRNA in the cells transfected

by pPrPwild is similar to that in wild-type mice. These results indicate that our newly established *in vitro* transient transfection system could reproduce the abnormal expression of PrPLP/Dpl in the ataxic lines of *Prnp*$^{0/0}$ mice in cultured cells by expression of EGFP fluorescent protein. Since pPrPtargeted lacks the *Prnp* sequences commonly targeted in the ataxic lines of *Prnp*$^{0/0}$ mice (Sakaguchi et al., 1995; Moore et al., 1999; Rossi et al., 2001), it is conceivable that the abnormal expression of PrPLP/Dpl in the ataxic lines of *Prnp*$^{0/0}$ mice is very likely due to deletion of a *cis*-element(s) present in the commonly targeted *Prnp* sequences.

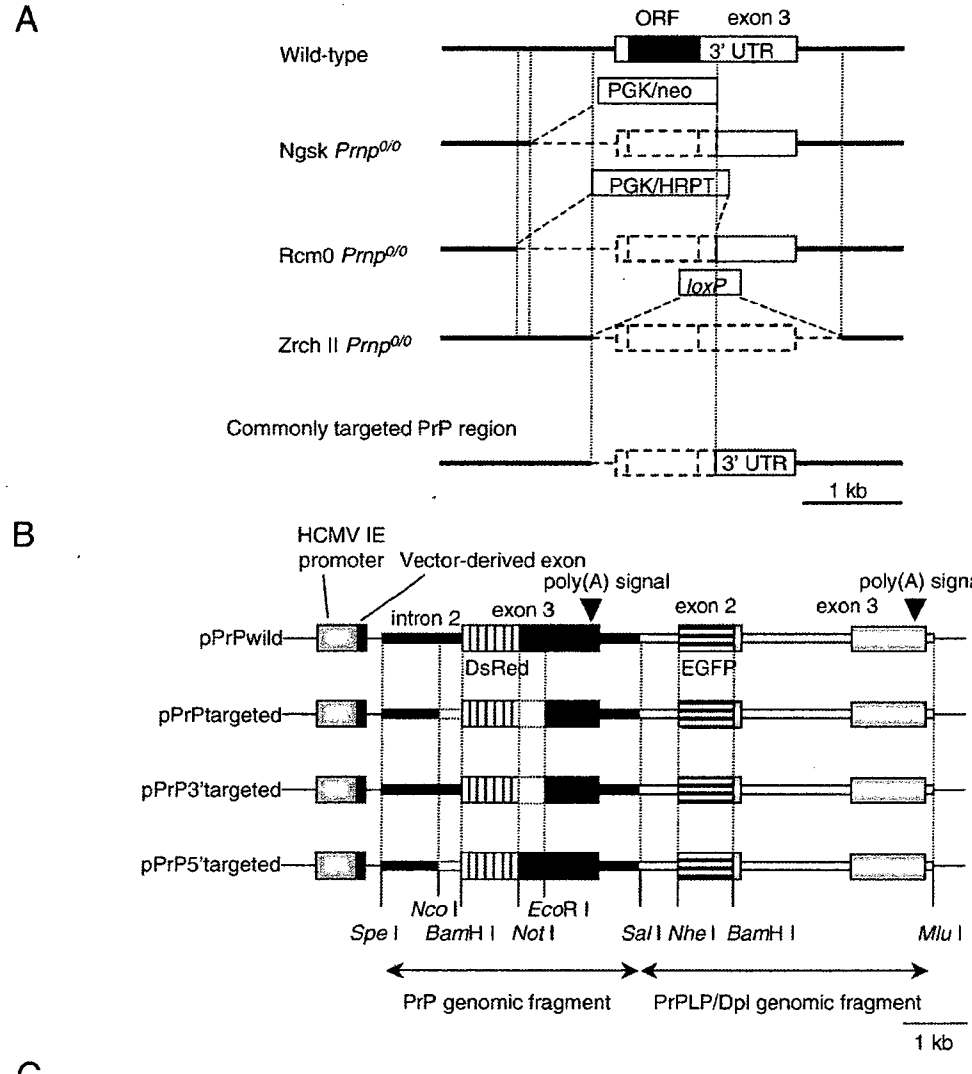

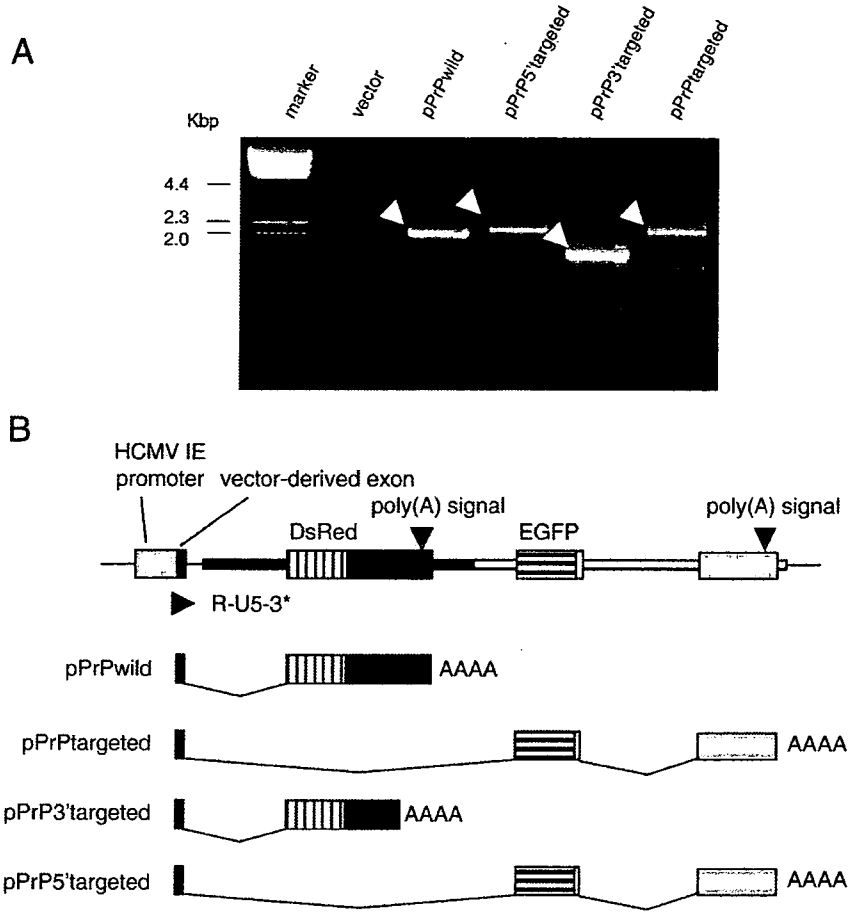

Fig. 2. (A) 3′ RACE of N2a cells 48 h after transient transfection of pPrPwild, pPrPtargeted, pPrP3′targeted, and pPrP5′targeted. Several distinct bands including one major band (indicated by arrow heads) are visible in each lane. (B) Schematic structures of the major transcripts expressed in the transfected N2a cells. These structures were determined on the basis of the DNA sequence of each major band. All poly(A) signals are native. AAAA indicates a poly(A) tail. R-U5-3* is a primer used for 3′ RACE.

3.2. Abnormal expression of PrPLP/Dpl assessed in the in vitro transient transfection system with vectors carrying various deletions in the upstream Prnp sequence

To employ our newly established *in vitro* system to investigate the genetic mechanism of the abnormal expression of PrPLP/Dpl in the ataxic lines of *Prnp*$^{0/0}$ mice, we constructed two other vectors, pPrP3′targeted and pPrP5′targeted. pPrP3′targeted lacks 450-bp of the *Prnp* 3′ UTR whereas pPrP5′targeted lacks 249-bp of intron 2 and 10-bp of the 5′ UTR (Fig. 1B). We transfected pPrP3′targeted and pPrP5′targeted into N2a cells. pPrP3′targeted expressed DsRed but not EGFP fluorescence in N2a cells 48 h after transfection (Fig. 1C). 3′ RACE and DNA sequencing showed that the major transcript expressed in these cells was composed of the vector-derived exon and the *Prnp* exon 3, similar to that in pPrPwild-transfected cells (Fig. 2A and B). This compositional similarity of the transcripts indicates that the pre-mRNAs expressed from pPrPwild and pPrP3′targeted are similarly processed in these transfected cells. Since pPrP3′targeted lacks the commonly targeted *Prnp* 3′ UTR, deletion of this part is unlikely to be involved in the

Fig. 1. (A) *Prnp* alleles in wild-type, Ngsk *Prnp*$^{0/0}$, Rcm0 *Prnp*$^{0/0}$, and Zrch II *Prnp*$^{0/0}$ mice. In Ngsk *Prnp*$^{0/0}$ mice, a 2.1-kb *Prnp* genomic DNA comprising 900-bp of intron 2, 10-bp of the 5′ UTR, an entire PrP ORF, and 450-bp of the 3′ UTR was replaced with a neomycin cassette (Sakaguchi et al., 1995). A similar part of *Prnp* was targeted in Rcm0 *Prnp*$^{0/0}$ mice (Moore et al., 1999). In Zrch II *Prnp*$^{0/0}$ mice, the *Prnp* genomic region consisting of 250-bp of intron 2, the entire exon 3, and 600-bp of the downstream intervening sequence was deleted (Rossi et al., 2001). Thus, 250-bp of intron 2 and a subsequent part of exon 3 including 10-bp of the 5′ UTR, the ORF, and 450-bp of the 3′ UTR are commonly targeted. (B) Schematic structures of the expression vectors, pPrPwild, pPrPtargeted, pPrP3′targeted, and pPrP5′targeted. pPrPwild was constructed by ligation of a PrP genomic fragment, including part of intron 2, exon 3, and the 3′ downstream sequence, and a PrPLP/Dpl genomic fragment including a part of intron 1, exon 2, intron 2, exon 3 and the 3′ downstream sequence in tandem under the control of the HCMV IE promoter. Each exon 3 contains a native poly(A) signal. The ORFs for PrP and PrPLP/Dpl are replaced with those for DsRed and EGFP, respectively. pPrPtargeted lacks the same part of *Prnp* as in the ataxic lines of *Prnp*$^{0/0}$ mice as indicated by the dotted square. pPrP3′targeted lacks 450-bp of the PrP 3′ UTR and pPrP5′targeted lacks 250-bp of intron 2 and 10-bp of the 5′ UTR. (C) Fluorescent microscopic photographs of mouse neuroblastoma N2a cells 48 h after transient transfection with pPrPwild, pPrPtargeted, pPrP3′targeted, and pPrP5′targeted.

abnormal regulation of *Prnd* in the ataxic lines of *Prnp*$^{0/0}$ mice. In contrast, pPrP5′targeted showed green EGFP fluorescence in the cells (Fig. 1B) and expressed the major transcript consisting of the vector-derived exon that was aberrantly spliced to the downstream *Prnd* exon 2 (Fig. 2A and B), similar to pPrPtargeted (Fig. 1B). These results indicate that our newly established *in vitro* transient transfection system is highly feasible to investigate the genetic mechanism of the abnormal expression of PrPLP/Dpl in the ataxic lines of *Prnp*$^{0/0}$ mice. pPrP5′targeted lacks 249-bp of intron 2 and 10-bp of the 5′ UTR. Thus, it is suggested that deletion of either 249-bp of intron 2 or 10-bp of the 5′ UTR or both in *Prnp* is responsible for the abnormal expression of downstream *Prnd* in the ataxic lines of *Prnp*$^{0/0}$ mice.

We further employed the *in vitro* system with several additional vectors, which were constructed by sequentially deleting 249-bp of intron 2 from the 5′ end. pPrPint2(-3) possesses only 3-bp of intron 2, including a splice acceptor of dinucleotides AG, and the subsequent 10-bp of the 5′ UTR (Fig. 3A). N2a cells transfected by this vector expressed EGFP, similar to those of pPrPtargeted and pPrP5′targeted (Fig. 3B), indicating that deletion of *Prnp* intron 2 is responsible for the abnormal expression of *Prnd*-coding exon in the transfected cells. In contrast, pPrPint2(-26) and pPrPint2(-50), containing 3′ 26- and 50-bp of intron 2, respectively, together with 10-bp of the 5′ UTR, exhibited DsRed signals in the cells (Fig. 3A and B). These results indicate that the unsuccessful cleavage/polyadenylation-mediated abnormal expression of *Prnd*-coding exon in the transfected cells is attributable to deletion of at least the 3′ 26-bp of *Prnp* intron 2. It is also suggested that lack of the same sequence in *Prnp* is responsible for the abnormal expression of PrPLP/Dpl in the ataxic lines of *Prnp*$^{0/0}$ mice.

3.3. The in vitro transient transfection system visualizes the functional disconnection of the pre-mRNA machineries underlying the abnormal expression of PrPLP/Dpl

Within the 26-bp intronic sequence, various elements important for pre-mRNA splicing, including a splice branch point, a polypyrimidine tract, and a splice acceptor are present. To investigate whether disruption of these elements could be involved in the impairment of pre-mRNA cleavage/polyadenylation at the end of *Prnp* leading to EGFP expression, we introduced various point mutations into the splice acceptor and/or the branch point in pPrPint2(-26). pPrPint2(-26)AG, carrying a G to T mutation in both the authentic splice acceptor AG and the adjacent downstream cryptic AG in the 5′ UTR, showed expression of EGFP in the cells (Fig. 4A and B). pPrPint2(-26)AGBr2× including mutations in all of these branch points and splice acceptors similarly expressed EGFP in the cells (Fig. 4A and B). These results clearly indicate that disruption of the splice acceptor in *Prnp* intron 2 caused expression of the downstream EGFP-coding exon. In contrast, pPrPint2(-26)Br carries an A to T mutation at the authentic branch point and expressed DsRed in the transfected N2a cells (Fig. 4A and B). Similar DsRed expression was observed in the cells transfected by pPrPint2(-26)Br2×, which contained an additional A to G mutation at the 2-bp downstream cryptic branch point (Fig. 4A and B). Therefore,

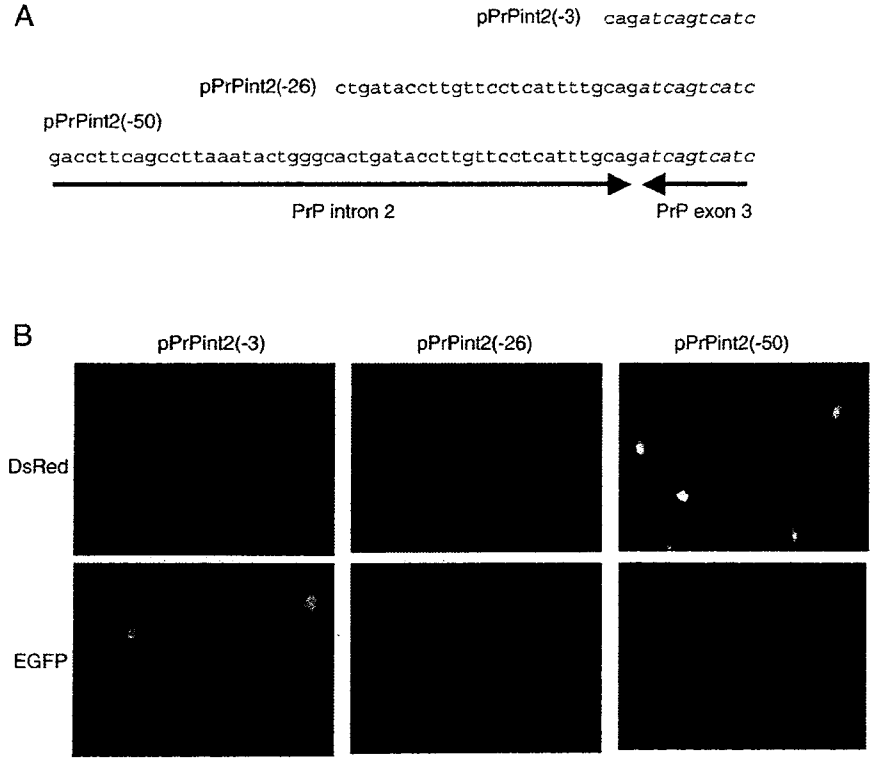

Fig. 3. (A) Nucleotide sequences of PrP intron 2 and exon 3 in pPrPint2(-3), pPrPint2(-26), and pPrPint2(-50). Italic letters are nucleotides in exon 3. (B) Fluorescent microscopic photographs of N2a cells 48 h after transient transfection with pPrPint2(-3), pPrPint2(-26), and pPrPint2(-50).

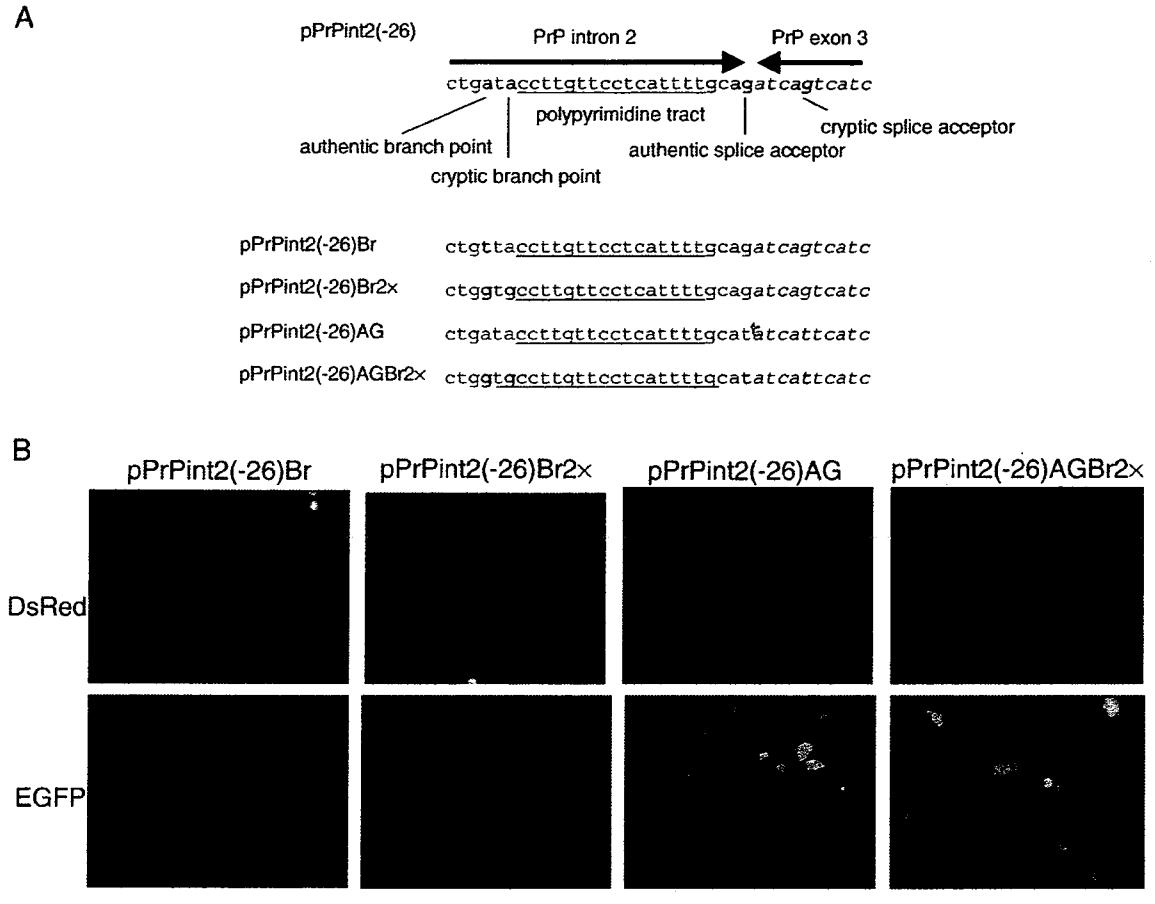

Fig. 4. (A) Point mutations introduced in the splice elements of pPrPint2(-26)Br, pPrPint2(-26)Br2×, pPrPint2(-26)AG, and pPrPint2(-26)AGBr2×. Nucleotide sequences in PrP intron 2 and exon 3 of pPrPint2(-26) are shown, including authentic and cryptic branch points, splice acceptors and a polypyrimidine tract. Mutated nucleotides are shown in bold letters. (B) Fluorescent microscopic photographs of N2a cells 48 h after transient transfection with pPrPint2(-26)Br, pPrPint2(-26)Br2×, pPrPint2(-26)AG, and pPrPint2(-26)AGBr2×.

it appears that lack of the functional branch point is unlikely to be involved in the abnormal expression of *Prnd*. However, pPrPint2(-3), which possesses the splice acceptor but lacks the branch point and polypyrimidine tract, expressed EGFP in N2a cells (Fig. 3B), indicating that deletion of the branch point or polypyrimidine tract might also be responsible for the expression of EGFP. It is thus possible that the expression of DsRed in the cells transfected by pPrPint2(-26)Br or pPrPint2(-26)Br2× is due to the presence of other functional cryptic branch points. Taken together, these results indicate that collapse in the integrity of splicing machineries could be responsible for the expression of EGFP in the cells by causing the impaired cleavage/polyadenylation of pre-mRNA. It is recently believed that splicing of the terminal intron is functionally linked to the cleavage/polyadenylation of pre-mRNA during transcription (Steinmetz, 1997; Proudfoot et al., 2002; Kornblihtt et al., 2004). It is therefore very likely that the functional disconnection of pre-mRNA machineries, in particular those of splicing and cleavage/polyadenylation, underlies the abnormal expression of PrPLP/Dpl in the ataxic lines of *Prnp*$^{0/0}$ mice. More importantly, these results indicate that our established *in vitro* transient transfection system is very useful to easily detect the functional disconnection of the pre-mRNA machineries from the expression of the EGFP fluorescent protein under fluorescence microscopy.

Splicing is mediated by a large molecular complex, splicesome, consisting of small nuclear ribonucleoproteins (snRNPs) and non-RNP splicing factors of a SR protein family (Proudfoot et al., 2002). The cleavage/polyadenylation of pre-mRNA is also regulated by various factors, including poly(A) polymerase (PAP), cleavage/polyadenylation specificity factor (CPSF), and cleavage stimulatory factor (Wahle and Ruegsegger, 1999; Proudfoot et al., 2002). U2AF is a dimeric splicing factor, interacting with the splice acceptor and polypyrimidine tract and helping recruit the U2 snRNP to the branch point together with a branch point binding protein (Vagner et al., 2000). It has been shown that PAP can interact with the large subunit of U2AF, U2AF65, and stimulate pre-mRNA splicing *in vivo* (Vagner et al., 2000). It was also reported that U2AF65 increased 3′-end cleavage efficiency (Millevoi et al., 2002). It is therefore conceivable that U2AF is a key molecule functionally connecting splicing and cleavage/polyadenylation. However, the molecular mechanism of how the pre-mRNA machineries are functionally connected to each other remains to be investigated.

Thus, our newly established *in vitro* transient transfection system might be employed to investigate the mechanism of the functional connection between the pre-mRNA machineries.

Recently, it has been shown that some viral proteins can disturb the function of pre-mRNA machineries by interacting with their components. Influenza virus NS1 protein was shown to inhibit cleavage/polyadenylation processes of cellular pre-mRNA by interacting with the 30 kDa subunit of CPSF (Nemeroff et al., 1998). Shimizu et al. subsequently reported that transcripts for the major heat shock protein HSP70, and β-actin were elongated due to the insufficient cleavage of these corresponding pre-mRNAs in influenza virus-infected cells (Shimizu et al., 1999). It was also shown that Epstein–Barr virus protein nuclear antigen 5 could inhibit cleavage/polyadenylation of cellular pre-mRNA (Dufva et al., 2002), and that human cytomegalovirus infection altered splicing and polyadenylation of cellular pre-mRNA (Adair et al., 2004). Interestingly, it was shown that Tgat, an oncogenic protein, was newly generated probably due to the impaired pre-mRNA processing in adult T-cell leukemia, the disease caused by human T-cell leukemia virus (Yoshizuka et al., 2004). Therefore, our newly established system may also be applied to elucidation of the molecular pathogenesis of pathological conditions.

3.4. Conclusions

In this study, we newly established an *in vitro* transient transfection system in which the functional disconnection of the pre-mRNA machineries could easily be detected by the expression of EGFP fluorescent protein under fluorescence microscopy. Employing this system, we showed that the abnormal expression of PrPLP/Dpl in ataxic lines of *Prnp*$^{0/0}$ mice can be visualized by expression of the green fluorescence protein EGFP in cultured cells, and identified that the abnormal expression of PrPLP/Dpl is probably due to functional disconnection between the pre-mRNA machineries, in particular those of splicing and cleavage/polyadenylation. Therefore, our newly established *in vitro* system might be useful to investigate the molecular mechanisms of the functional connection between the pre-mRNA machineries in normal and pathological conditions.

Acknowledgement

This study was supported in part by a Research on Specific Diseases grant from the Ministry of Health, Labour and Welfare, Japan.

References

Adair, R., Liebisch, G.W., Su, Y., Colberg-Poley, A.M., 2004. Alteration of cellular RNA splicing and polyadenylation machineries during productive human cytomegalovirus infection. J. Gen. Virol. 85, 3541–3553.

Anderson, L., Rossi, D., Linehan, J., Brandner, S., Weissmann, C., 2004. Transgene-driven expression of the Doppel protein in Purkinje cells causes Purkinje cell degeneration and motor impairment. Proc. Natl. Acad. Sci. U. S. A. 101, 3644–3649.

Behrens, A., et al., 2002. Absence of the prion protein homologue Doppel causes male sterility. EMBO J. 21, 3652–3658.

Bueler, H., et al., 1992. Normal development and behaviour of mice lacking the neuronal cell-surface PrP protein. Nature 356, 577–582.

Dufva, M., Flodin, J., Nerstedt, A., Ruetschi, U., Rymo, L., 2002. Epstein–Barr virus nuclear antigen 5 inhibits pre-mRNA cleavage and polyadenylation. Nucleic Acids Res. 30, 2131–2143.

Kornblihtt, A.R., de la Mata, M., Fededa, J.P., Munoz, M.J., Nogues, G., 2004. Multiple links between transcription and splicing. RNA 10, 1489–1498.

Li, A., et al., 2000a. Identification of a novel gene encoding a PrP-like protein expressed as chimeric transcripts fused to PrP exon 1/2 in ataxic mouse line with a disrupted PrP gene. Cell. Mol. Neurobiol. 20, 553–567.

Li, A., et al., 2000b. Physiological expression of the gene for PrP-like protein, PrPLP/Dpl, by brain endothelial cells and its ectopic expression in neurons of PrP-deficient mice ataxic due to Purkinje cell degeneration. Am. J. Pathol. 157, 1447–1452.

Manson, J.C., Clarke, A.R., Hooper, M.L., Aitchison, L., McConnell, I., Hope, J., 1994. 129/Ola mice carrying a null mutation in PrP that abolishes mRNA production are developmentally normal. Mol. Neurobiol. 8, 121–127.

Millevoi, S., Geraghty, F., Idowu, B., Tam, J.L., Antoniou, M., Vagner, S., 2002. A novel function for the U2AF 65 splicing factor in promoting pre-mRNA 3′-end processing. EMBO Rep. 3, 869–874.

Moore, R.C., et al., 1999. Ataxia in prion protein (PrP)-deficient mice is associated with upregulation of the novel PrP-like protein Doppel. J. Mol. Biol. 292, 797–817.

Moore, R.C., et al., 2001. Doppel-induced cerebellar degeneration in transgenic mice. Proc. Natl. Acad. Sci. U. S. A. 98, 15288–15293.

Nemeroff, M.E., Barabino, S.M., Li, Y., Keller, W., Krug, R.M., 1998. Influenza virus NS1 protein interacts with the cellular 30 kDa subunit of CPSF and inhibits 3′end formation of cellular pre-mRNAs. Mol. Cell 1, 991–1000.

Proudfoot, N.J., Furger, A., Dye, M.J., 2002. Integrating mRNA processing with transcription. Cell 108, 501–512.

Rossi, D., et al., 2001. Onset of ataxia and Purkinje cell loss in PrP null mice inversely correlated with Dpl level in brain. EMBO J. 20, 694–702.

Sakaguchi, S., et al., 1995. Accumulation of proteinase K-resistant prion protein (PrP) is restricted by the expression level of normal PrP in mice inoculated with a mouse-adapted strain of the Creutzfeldt–Jakob disease agent. J. Virol. 69, 7586–7592.

Sakaguchi, S., et al., 1996. Loss of cerebellar Purkinje cells in aged mice homozygous for a disrupted PrP gene. Nature 380, 528–531.

Shimizu, K., Iguchi, A., Gomyou, R., Ono, Y., 1999. Influenza virus inhibits cleavage of the HSP70 pre-mRNAs at the polyadenylation site. Virology 254, 213–219.

Steinmetz, E.J., 1997. Pre-mRNA processing and the CTD of RNA polymerase II: the tail that wags the dog? Cell 89, 491–494.

Vagner, S., Vagner, C., Mattaj, I.W., 2000. The carboxyl terminus of vertebrate poly(A) polymerase interacts with U2AF 65 to couple 3′-end processing and splicing. Genes Dev. 14, 403–413.

Wahle, E., Ruegsegger, U., 1999. 3′-End processing of pre-mRNA in eukaryotes. FEMS Microbiol. Rev. 23, 277–295.

Yamaguchi, N., Sakaguchi, S., Shigematsu, K., Okimura, N., Katamine, S., 2004. Doppel-induced Purkinje cell death is stoichiometrically abrogated by prion protein. Biochem. Biophys. Res. Commun. 319, 1247–1252.

Yoshizuka, N., et al., 2004. An alternative transcript derived from the trio locus encodes a guanosine nucleotide exchange factor with mouse cell-transforming potential. J. Biol. Chem. 279, 43998–44004.

Available online at www.sciencedirect.com
ScienceDirect
ELSEVIER
Biochemical and Biophysical Research Communications 355 (2007) 269–274
BBRC
www.elsevier.com/locate/ybbrc

Tgat, a Rho-specific guanine nucleotide exchange factor, activates NF-κB via physical association with IκB kinase complexes

Kenji Yamada [a,b], Ryozo Moriuchi [a,*], Tsuyoshi Mori [a], Eiko Okazaki [a], Tomoko Kohno [a], Takeshi Nagayasu [b], Toshifumi Matsuyama [a], Shigeru Katamine [a]

[a] *Department of Molecular Microbiology & Immunology, Nagasaki University Graduate School of Biomedical Sciences, 1-12-4 Sakamoto, Nagasaki 852-8523, Japan*

[b] *Division of Surgical Oncology, Department of Translational Medical Sciences, Nagasaki University Graduate School of Biomedical Sciences, Nagasaki, Japan*

Received 15 January 2007
Available online 2 February 2007

Abstract

Constitutive activity of NF-κB is associated with various human cancers including adult T-cell leukemia (ATL). In this study, we have found *Tgat* that activates NF-κB by screening a cDNA expression library derived from ATL cells. We previously identified *Tgat* as the oncogene, which consists of the Rho-guanine nucleotide exchange factor (Rho-GEF) domain and the unique C-terminal region, as a consequence of alternative splicing of the *Trio* transcript. Tgat activated the IKK activity by binding with the IκB kinase (IKK) complex. The Tgat mutants lacking the C-terminal region failed to associate with the IKK complex suggesting an essential role of the unique sequence. The mutation causing the loss of GEF activity also abolished the NF-κB activation. Moreover, co-expressed p100 was efficiently processed into p52 in the Tgat-expressing cells, suggesting the co-involvement of non-canonical pathway.

Keywords: NF-κB; Tgat; Rho-GTPase; Trio; HTLV-1; Tax; ATL

Accumulating evidences have indicated a role of NF-κB in tumorigenesis. A number of other viral proteins might be oncogenic interacting with IKK complex and cause NF-κB activation. For instance, the Epstein–Barr virus (EBV), implicated in lymphoid and epithelial malignancies such as Burkitt's lymphoma and Hodgkin's disease, post-transplant lymphoma, gastric carcinoma, and nasopharyngeal carcinoma, induces persistent NF-κB activation mediated by latent membrane protein 1 (LMP-1) and EBV nuclear antigen-2 (EBNA-2) [1,2]. Kaposi's sarcoma-associated herpes virus (KSHV), the causal agent of Kaposi's sarcoma, primary effusion B cell lymphomas, and multicentric Castleman's disease, has been shown to transform the infected cells through p21-activated kinase 1 (Pak 1) mediated NF-κB activation [3]. Another example is human T-lymphotropic virus type-1 (HTLV-1), which causes adult T-cell leukemia (ATL). The *pX* region of HTLV-1 encodes a transcriptional transactivator Tax, which activates expression of HTLV-1 long terminal repeat (LTR) through a DNA element that resembles the cellular cyclic AMP-regulated enhancer (CRE) [4]. The Tax also activates NF-κB, and the activation has been shown to be indispensable for transformation of rat fibroblasts *in vitro* [5]. However, Tax is barely detectable in ATL cells freshly isolated from patients. Tax expression in ATL cells is often abolished by genetic mutation in the *tax* gene, deletion of the 5′ LTR [6,7] or hyper-methylation of the promoter/enhancer region in 5′ LTR [8]. Moreover, the NF-κB subunits activated in the leukemic cells is different from those in

Abbreviations: NF-κB, nuclear factor-κB; HTLV-1, human T-lymphotropic virus type 1; ATL, adult T-cell Leukemia; Tgat, trio-related transforming gene in ATL tumor cells; GEF, guanine nucleotide exchange factor; IKK, IκB kinase.

* Corresponding author. Fax: +81 95 849 7060.
E-mail address: ryozo@nagasaki-u.ac.jp (R. Moriuchi).

0006-291X/$ - see front matter © 2007 Elsevier Inc. All rights reserved.
doi:10.1016/j.bbrc.2007.01.147

Tax-expressing cell lines; the NF-κB binding activity in ATL cells consists of p50/p65 heterodimer and p50/p50 homodimer, whereas Tax-expressing T-cell lines mostly of p50/c-Rel [9]. The molecular mechanism responsible for the constitutive NF-κB activation in ATL cells remains unknown.

In this study, we identify Tgat as the molecule with the potential to activate NF-κB by screening cDNA expression library derived from freshly isolated ATL cells. This report also demonstrates that the features of NF-κB activation by Tgat mimic those observed in ATL cells.

Materials and methods

DNA constructs. Methods of cDNA library construction and *Tgat* mutants (*Tgat*ΔC, *Tgat*PH2, and *Tgat*GEFdead) generation were as described previously [10]. For mutants construction, PCR-amplified DNA fragments encoding Rho-GEF domain were ligated into pDON-AI containing PH2 coding sequence of *Trio* gene. Site-directed mutagenesis was applied to construct *Tgat*GEFdead that lacked Rho-GEF activity. Nucleotide sequence of each construct was confirmed by DNA sequencing. pIL-2Rα-Luc contains the luciferase gene under the control of five tandem copies of the NF-κB binding sequence of the IL-2Rα gene (GGGAATCTCC).

Transient transfection of 293T cells and the NF-κB reporter gene assay. 293T cells, seeded at 5×10^4 cells per well 24 h prior to transfection, were transfected in 24-well plates by calcium phosphate co-precipitation. To analyze expression of the NF-κB-dependent reporter gene, pIL-2Rα-Luc or pNF-κB-Luc reporter plasmid, pDON-*Tgat* or its derivatives and RL-TK-Luc plasmid were co-transfected into 293T cells.

Oligonucleotides. The sequence of the oligonucleotide corresponding to the κB element from IL-2Rα gene was 5′-CAGTTGAGGGGAATCTCC CAGGC-3′. For competition study, oligonucleotide-containing mutant κB was used, and the sequence was 5′-CAGTTGAGatctATCTCCCA GGC-3′.

Electrophoretic mobility shift assay. To examine the NF-κB activity in 293T cells, an aliquot of the nuclear extracts was incubated in a reaction buffer (10 mM Hepes, pH 7.6, 50 mM KCl, 0.1 mM EDTA, 0.5 mM DTT, 0.25 mM PMSF, 10% glycerol, and 100 μg/ml poly(dI–dC)). In some cases, a 20-fold molar excess of unlabeled double-stranded oligonucleotide was added as a competitor. After a 10-min incubation on ice, an end-labeled double-stranded oligonucleotide containing the consensus NF-κB binding sequence was added to the reaction, which was then incubated for an additional 30 min at room temperature. The same oligonucleotide in the unlabeled form was used as the wild-type competitor. And the mutant competitor previously described was used. In some cases, the reactions were further incubated with anti-p50, anti-p65, anti-c-Rel, anti-p52 or anti-RelB Abs at room temperature for 30 min. The samples were analyzed by electrophoresis in a 5% non-denaturing polyacrylamide gel with 0.5× TBE buffer. The gels were dried and analyzed by autoradiography.

Immunoprecipitation and kinase assay. Cytoplasmic extracts prepared from equivalent number of cells were subjected to immunoprecipitation with anti-FLAG M2 affinity gel in TNT buffer (20 mM Tris–HCl, pH 7.5, 200 mM NaCl, 1% Triton X-100, 0.5 mM PMSF, 100 μM Na_3VO_4, 20 mM β-glycerophosphate, and one-hundredth volume of a protease inhibitor mixture). Immunoprecipitates were then washed three times with TNT buffer and three times with kinase reaction buffer (20 mM Hepes, pH 7.5, 10 mM $MgCl_2$, 50 mM NaCl, 100 μM Na_3VO_4, 20 mM β-glycerophosphate, 2 mM DTT, 20 μM ATP). Kinase reactions were performed for 30 min at 30 °C using 5 μCi of [γ-^{32}P]ATP and GST-IκBα (amino acids 1–72) as substrates. The reaction products were separated on 12% SDS polyacrylamide gels and revealed by autoradiography [11].

Immunoblotting (IB) and co-immunoprecipitation (Co-IP) assays. 293T cells were transfected with a HA-tagged *Tgat* construct or its mutants (5 μg) along with a IKK1 (5 μg) by calcium phosphate co-precipitation. At 48 h post-transfection, the cells were washed with 5 ml PBS and whole-cell lysates were harvested using radioimmuno-precipitation buffer (50 mM Tris–HCl, pH 7.4, 150 mM NaCl, 1% Nonidet P-40, 0.5% sodium deoxycholate, 1 mM EDTA, 1 mM phenylmethylsulfonyl fluoride, 1 mM DTT, and one-hundredth volume of a protease inhibitor mixture). The cell lysates were then incubated with anti-IKKs Abs for 1 h and with 20 μl of protein G-Sepharose beads for another 2 h. The beads were washed three times with radioimmuno-precipitation buffer and bound proteins were eluted in 1× SDS sample buffer and subjected to SDS–PAGE and Western blot analysis using anti-HA mouse monoclonal Abs.

Results

Identification of Tgat capable of activating NF-κB in 293T cells by expression cDNA cloning

We sorted 293T-κB-EGFP cells showing NF-κB activity after transfection with a cDNA library derived from ATL cells and isolated the cDNAs capable of activating NF-κB (Supplementary Fig. S1). Two rounds of FACS enrichment and subsequent sib selection finally identified 15 positive clones. The clone 33-44-57-34 conferring fluorescence-activation on the transfected cells, was *Tgat* (trio-related transforming gene in ATL tumor cells), which we previously reported as a novel transforming gene activated by alternative RNA splicing between a part of Trio gene encoding Rho-GEF and a novel exon located downstream of the last exon of *Trio* [10]. Sequence analysis revealed that others, including clone 33-44-57-12 which gave very intense fluorescent signals in transfected 293T cells, encoded EGFP under the CMV promoter probably due to the artificial homologous recombination between the integrated κB-EGFP sequence and the promoter region of the transfected vector.

Tgat activates both canonical and non-canonical pathways

To confirm the activation NF-κB by *Tgat*, the cDNA was co-transfected with a reporter plasmid with the luciferase gene under the κB enhancer. To rule out selective failure due to the subtle sequence heterogeneity of κB enhancers, we used two independent reporter plasmids, pIL-2Rα-Luc containing the κB enhancer from IL-2Rα chain (Fig. 1A) and pNF-κB-Luc (Supplementary Fig. S2). As shown in Fig. 1A, the level of luciferase activity detected in *Tgat*-transfected cells co-transfected with pIL-2Rα-Luc was about 2.5 times higher than that of empty vector-transfected cells with statistical significance ($p < 0.01$, ANOVA). The level of pNF-κB-Luc transactivation was less than that by HTLV-I Tax, but Tgat transactivated pIL-2Rα-Luc at similar level as Tax. Next the nuclear extracts of cells were subjected to EMSA. A small amount of NF-κB-specific protein/DNA complexes detectable in nuclear extracts of vector-transfected cells drastically increased in *Tgat*-transfected cells. The specificity of the binding was confirmed by competition with an excess amount of wild-type but not mutant oligonucleotides (Fig. 1B). NF-κB involved in the DNA binding in the *Tgat*-transfected cells predominantly consisted of p50 and

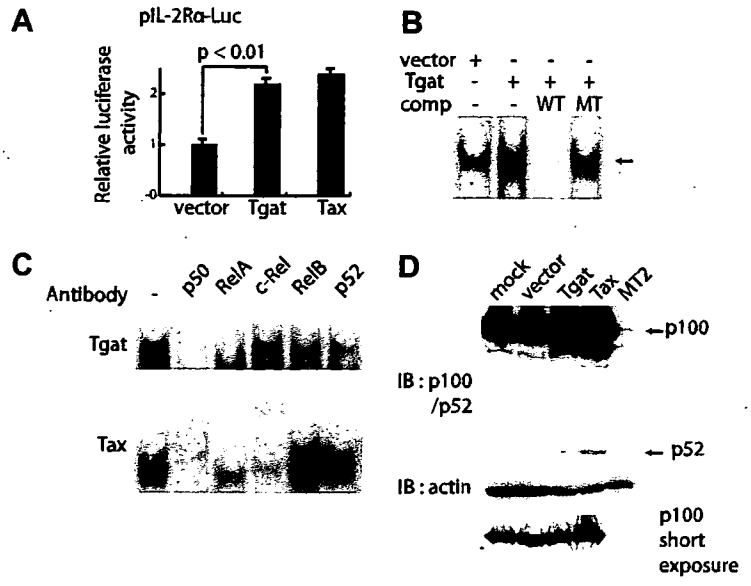

Fig. 1. Tgat and Tax express NF-κB-related activities. (A) 293T cell lines were transfected with 50 ng of a reporter plasmid containing the luciferase gene fused to five repeats of the κB motif of the IL-2Rα gene and enhancerless promoter of thymidine kinase (pIL-2Rα-Luc) along with combinations of 10 ng of the cDNA expression plasmids and 0.5 ng of the internal control plasmid (pRL-TK-Luc). After 48 h, relative luciferase activity was determined. The results shown are averages of three independent experiments with SE bars. The relative luciferase activities in *Tgat* or *tax*-transfected cells were increased more than 2.5-fold compared to control ($P < 0.01$). The data was analyzed statistically by the Scheffe's F test. (B) Nuclear extracts (10 μg) from 293T cell line were assessed for activation of NF-κB by EMSA. The nuclear extracts were incubated with a ^{32}P end-labeled oligonucleotide, followed by gel electrophoresis. The black arrow indicates the NF-κB-containing complex. Nuclear extracts from 293T transfected with *Tgat* were incubated with the labeled NF-κB probe, in the presence of competitors. The unlabeled oligonucleotide (lane 3) or the mutant NF-κB oligonucleotide (lane 4) was added as a competitor in a 20-fold molar excess to the binding reaction. (C) Nuclear extracts (10 μg) from 293T cell transfected with *Tgat* (top) or *tax* (bottom) were pre-incubated with NF-κB subunit-specific antibody, against p50, RelA, c-Rel, RelB or p52 as indicated above each lane, before the addition of radiolabeled probe. (D) 293T cells were transfected with 3.3 μg of pDON/SfiI vector, pDON-*Tgat* or pDON-*tax* together with 3.3 μg of pCn100, and lysed in 1× SDS sample buffer at 15 h post-transfection. Whole cell extracts were subjected to immunoblot analysis with anti-p52 antibody. The same quantity of the same extracts was used for detection of actin by immunoblotting.

RelA subunits, because antibodies against p50 and RelA efficiently inhibited formation of the complex (Fig. 1C). Moreover, treatment of anti-RelB and anti-p52 antibodies to a lesser extent but significantly decreased the complex in the *Tgat*-transfected cells, suggesting that Tgat may activate NF-κB through not only canonical but also non-canonical pathway. On the other hand, activated NF-κB in the *tax*-transfected cells were mainly composed of p50 and c-Rel (Fig. 1C), as previously reported. Non-canonical pathway of NF-κB activation involves the processing of NF-κB2 p100 to generate p52 [11]. To confirm the involvement of Tgat in p100 processing, we expressed p100 in 293T cells together with *Tgat* or *tax*. Polyclonal antibodies to p100/p52 visualized p52 on a Western blot of whole cell lysates of *Tgat*-transfected cells (Fig. 1D, lane 3) as well as Tax-transfected cells and Tax-positive HTLV-1-transformed lymphoid cells, MT-2, but p52 was barely detectable in those of untransfected and vector-transfected 293T cells.

Both Rho-GEF activity and the C-terminal unique sequence of Tgat are necessary for NF-κB activation

Tgat protein contains the Rho-GEF domain followed by the unique 15 amino acid sequence at the carboxyl terminus. In order to elucidate the role of each region, transactivation potentials of the Tgat mutants, TgatΔC andTgatPH2 lacking the C-terminal unique region and TgatGEFdead encoding non-functional GEF [10], were examined. As shown in Fig. 2, luciferase activity detected in the cells transfected with *Tgat*ΔC, *Tgat*PH2, and *Tgat*GEFdead was decreased to the level similar to that of vector-transfected cells. Treatment of *Tgat*-transfected cells with 20 μM Y-27632, a pharmacological inhibitor of ROCK (Rho-associated kinase), also reduced the luciferase activity at the level similar to the control or *Tgat* mutants-transfected cells.

IKK1, IKK2, and IκBα mediate Tgat activation of NF-κB

In order to elucidate mechanisms of the Tgat-induced activation of canonical pathway, we examined the effects dominant-negative mutants of IκBα and IKKs. The elevated luciferase activities in *Tgat* or *tax*-transfected cells were significantly inhibited by co-expression of IκBαM (Fig. 3A) as well as dnIKK1 and dnIKK2 (Fig. 3B). We next assessed the kinase activity of IKK complex in the *Tgat*-transfected cells using *in vitro* kinase assays. Flag-epitope-tagged IKK2 was expressed alone or in combination with *Tgat* or *tax*. Then Flag-IKK2 was immunoprecipitated

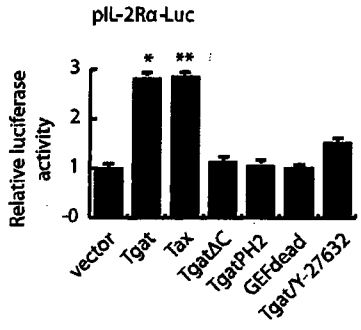

Fig. 2. NF-κB transcriptional activity of Tgat and its mutants in 293T cell line. Cells were co-transfected with pIL-2Rα-Luc (50 ng) and 10 ng *Tgat* or its mutant expression vector, together with 5 ng of the vector control plasmid (pRL-TK-Luc). After 48 h, relative luciferase activity was determined. The results shown are averages of three independent experiments with SE bars (*,**$P < 0.01$).

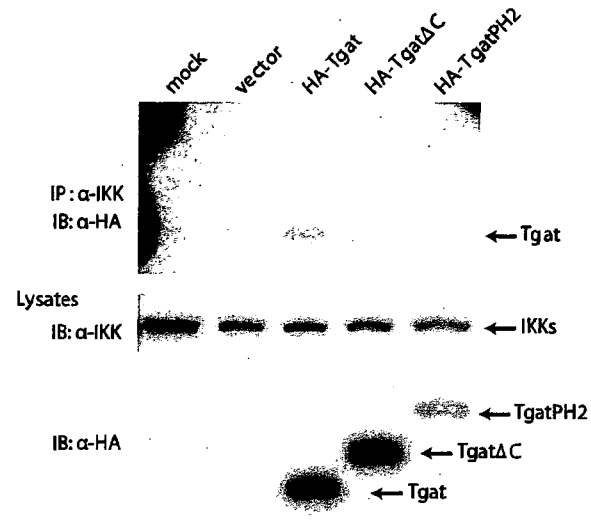

Fig. 4. Tgat interacts with IKK complex by its C-terminal region. 293T cells were transfected with a HA-tagged *Tgat* construct or its mutants. Polyclonal anti-IKKs antibody was used for immunoprecipitation (IP) and the immunoprecipitates were subjected to SDS–PAGE followed by Western blot analysis using anti-HA antibody.

from the cell lysates, one portion of the immunoprecipitates was used for *in vitro* phosphorylation assays with GST-IκBα as a substrate and the remainder was subjected to immunoblotting for detection of immunoprecipitated Flag-IKK2. The anti-Flag antibody precipitated roughly equivalent amounts of Flag-IKK2 from all the cell lysates (Fig. 3C, bottom). On the other hand, the levels of phosphorylation of GST-IκBα and autophosphorylation of Flag-IKK2 by *in vitro* kinase assay were about five times more in both *Tgat*- and *tax*-transfected cells, compared with those of the control cells (Fig. 3C, top).

Unique C-terminal region of Tgat is indispensable to the physical interaction with the IKK complex

To investigate whether the Tgat protein would physically interact with the IKK complex, Co-IP assay was performed (Fig. 4). The polyclonal anti-IKKs antibody precipitated endogenous IKKs together with HA-tagged Tgat but not TgatΔC and TgatPH2 from the lysates of transfected 293T cells. Flag-tagged IKKs were detectable in the anti-myc immunoprecipitates from the myc-Tgat-expressing cell lysates, but not from those of myc-TgatΔC and -TgatPH2 expressor (Supplementary Fig. S3). Interestingly, Flag-IKKs were precipitated with another Tgat mutant, TgatGEFdead, which preserves the C-terminal region but lacks GEF activity. These results suggest that

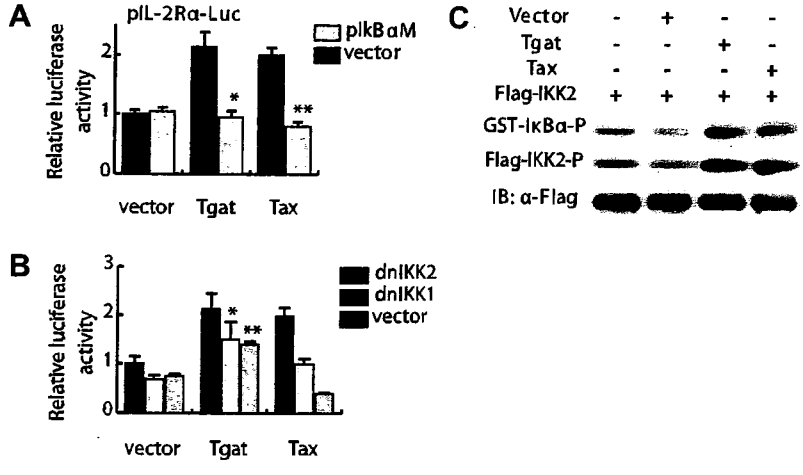

Fig. 3. IκBαM, DN-IKK1, and DN-IKK2 impaired Tgat activation of NF-κB in 293T. (A) 293T cells transfected with vector, pDON-*Tgat* (Tgat) or pDON-*tax* (Tax) and pIκBαM along with pIL-2Rα-Luc and pRL-TK-Luc. (B) 293T cells transfected with vector, pDON-*Tgat* (Tgat) or pDON-*tax* (Tax) and pDN-IKK1 or pDN-IKK2 along with pIL-2Rα-Luc and pRL-TK-Luc. The cells were harvested and lysed in lysis buffer 48 h after transfection. The cellular extracts were subjected to reporter gene assay. The κB-dependent luciferase activity was normalized based on the *Renilla* luciferase activity. The values shown are means from three separate transfections with SE bars (*,** $p < 0.01$). (C) Cytoplasmic extracts prepared from equivalent numbers of cells were immunoprecipitated with a FLAG specific monoclonal antibody and subjected to *in vitro* kinase assay using GST-IκBα as a substrate or to immunoblotting for detection of FLAG-IKK2 in the precipitates with a FLAG-specific monoclonal antibody.

the Tgat protein physically associates with IKKs via its carboxyl terminus and activates NF-κB.

Discussion

In this study, we identified Tgat as a potent stimulator of NF-κB by screening ATL-derived cDNA library. Both Rho-GEF activity and C-terminal unique region of Tgat were required for the NF-κB activation. Tgat physically associates with the IKK complex and its mutants lacking the unique C-terminal region but preserving the potential to activate cellular Rho-GTPase [10] failed to associate with IKKs and activate NF-κB. Dominant-negative mutants of IKK-1 and -2 abolish the NF-κB activation, suggesting the essential role of the interaction between Tgat and IKK complex. Interestingly, Tgat enhances the processing of p100 to p52, suggesting the co-involvement of non-canonical pathway of NF-κB activation. The alternative form of Rho-GEF, Tgat, would provide novel mechanisms to link the small G-protein cascade to transcription factor(s).

Tgat was originally identified in a cDNA library derived from fresh ATL cells. The *Tgat* mRNA was detectable in ATL cells and tissues, in contrast to the undetectable level in normal lymphocytes, suggesting some roles of Tgat in the malignant phenotype of ATL. Constitutive NF-κB activity is considered to be essential for the survival of ATL cells because pharmacological inhibitors of NF-κB or super-repressor form of IκBα induces apoptosis of the cells [11]. A number of investigations about oncoprotein Tax encoded by HTLV-1 have been performed to understand the mechanism by which HTLV-1 transforms human T-cells or contributes to the establishment of HTLV-1-associated inflammatory disorders. Tax is a well-known NF-κB activator and responsible for trans-activation or trans-repression of a variety of cellular genes coding cytokines and regulators of cell cycles, DNA repair or apoptosis. However, Tax is hardly implicated to the constitutive NF-κB activity in ATL cells, since Tax expression is usually undetectable in fresh ATL cells.

It has been reported that Tax binds to not only NF-κB members such as RelA, p50, and p52 but also IκBs including IκBα, p105, and p100 [12–15]. Tax is, however, incapable of direct activation of NF-κB via the interaction with NF-κB or IκB members. It has become apparent after the identification of IKK that Tax activation of NF-κB is mediated by IKK leading to IκB degradation and nuclear translocation of NF-κB [16–19]. Moreover, O'Mahony et al. has reported that IKK1 and IKK2 play the essential role for Tax-induced NF-κB activation; the former is involved in phosphorylation of RelA, the latter in the nuclear translocation of the canonical NF-κB [20]. We demonstrate here that Tgat likewise activates IKK2 followed by the IκBα degradation and RelA/p50 nuclear translocation. It is also suggested that IKK1 contributes to the Tgat activation of NF-κB judging from the result of reporter assay using dominant negative form of IKK1. This is supported by the facts that small amounts of RelB/p52 can be detected in the activated NF-κB and Tgat induces p100-processing leading to p52 production. Thus, Tgat seems to target the multiple axes of the NF-κB signaling network by stimulating different IKK components as well as Tax. Interestingly, however, RelA/p50 nuclear translocation is mainly induced by Tgat whereas c-Rel/p50 by Tax [21]. It was reported that NF-κB DNA-binding activity in primary ATL cells and Tax-negative T-cell lines contained RelA/p50 [9]. Aberrant expression of p52 was also demonstrated in Tax-negative ATL cell lines [11]. In this regard, the features of NF-κB activation provoked by Tgat rather than Tax are close to those observed in ATL cells.

It is now clear that NF-κB plays pivotal roles for survival of ATL cells and the constitutive NF-κB activity is thus a potential target to develop therapeutics of ATL. On the other hand, NF-κB plays a variety of physiological functions, in particular, in the immune system. Drugs, whose effects are restricted to a cancer-specific pathway of NF-κB activation, if present, are ideal for clinical application. An agent that blocks the physical interaction between Tgat and IKK complex may be beneficial in therapy of ATL, although the mechanisms of Tax-independent NF-κB activation in ATL cells should be investigated more extensively.

Acknowledgments

We Dr. S. Yamaoka (Tokyo Medical and Dental University) for pcDNA3GVSV-IKK1DN, pcDNA3GVSV-IKK2DN, and pCn-p100, and are also grateful to Dr. H. Nakano (Juntendo University) for pCR-Flag-IKK1 and pCR-Flag-IKK2. This work was supported by grants from the Ministry of Education, Culture, Sports, Science and Technology of Japan to R.M.

Appendix A. Supplementary data

Supplementary data associated with this article can be found, in the online version, at doi:10.1016/j.bbrc.2007.01.147.

References

[1] G. Mosialos, The role of Rel/NF-kappa B proteins in viral oncogenesis and the regulation of viral transcription, Semin. Cancer Biol. 8 (1997) 121–129.
[2] N. Saito, G. Courtois, A. Chiba, N. Yamamoto, T. Nitta, N. Hironaka, M. Rowe, S. Yamaoka, Two carboxyl-terminal activation regions of Epstein–Barr virus latent membrane protein 1 activate NF-kappaB through distinct signaling pathways in fibroblast cell lines, J. Biol. Chem. 278 (2003) 46565–46575.
[3] D. Dadke, B. Fryer, E. Golemis, J. Field, Activation of p21-activated kinase 1-nuclear factor kappaB signaling by Kaposi's sarcoma-associated herpes virus G protein-coupled receptor during cellular transformation, Cancer Res. 63 (2003) 8837–8847.
[4] R. Kwok, M. Laurance, J. Lundblad, P. Goldman, H. Shih, L. Connor, S. Marriott, R. Goodman, Control of cAMP-regulated enhancers by the viral transactivator Tax through CREB and the co-activator CBP, Nature 380 (1996) 642–646.

[5] S. Yamaoka, H. Inoue, M. Sakurai, T. Sugiyama, M. Hazama, T. Yamada, M. Hatanaka, Constitutive activation of NF-kappa B is essential for transformation of rat fibroblasts by the human T-cell leukemia virus type I Tax protein, EMBO J. 15 (1996) 873–887.
[6] Y. Furukawa, R. Kubota, M. Tara, S. Izumo, M. Osame, Existence of escape mutant in HTLV-I tax during the development of adult T-cell leukemia, Blood 97 (2001) 987–993.
[7] S. Okazaki, R. Moriuchi, N. Yosizuka, K. Sugahara, T. Maeda, I. Jinnai, M. Tomonaga, S. Kamihira, S. Katamine, HTLV-1 proviruses encoding non-functional TAX in adult T-cell leukemia, Virus Genes 23 (2001) 123–135.
[8] S. Takeda, M. Maeda, S. Morikawa, Y. Taniguchi, J. Yasunaga, K. Nosaka, Y. Tanaka, M. Matsuoka, Genetic and epigenetic inactivation of tax gene in adult T-cell leukemia cells, Int. J. Cancer 109 (2004) 559–567.
[9] N. Mori, M. Fujii, S. Ikeda, Y. Yamada, M. Tomonaga, D.W. Ballard, N. Yamamoto, Constitutive activation of NF-kappaB in primary adult T-cell leukemia cells, Blood 93 (1999) 2360–2368.
[10] N. Yoshizuka, R. Moriuchi, T. Mori, K. Yamada, S. Hasegawa, T. Maeda, T. Shimada, Y. Yamada, S. Kamihira, M. Tomonaga, S. Katamine, An alternative transcript derived from the trio locus encodes a guanosine nucleotide exchange factor with mouse cell-transforming potential, J. Biol. Chem. 279 (2004) 43998–44004.
[11] N. Hironaka, K. Mochida, N. Mori, M. Maeda, N. Yamamoto, S. Yamaoka, Tax-independent constitutive IkappaB kinase activation in adult T-cell leukemia cells, Neoplasia 6 (2004) 266–278.
[12] H. Hirai, J. Fujisawa, T. Suzuki, K. Ueda, M. Muramatsu, A. Tsuboi, N. Arai, M. Yoshida, Transcriptional activator Tax of HTLV-1 binds to the NF-kappa B precursor p105, Oncogene 7 (1992) 1737–1742.
[13] J. Lanoix, J. Lacoste, N. Pepin, N. Rice, J. Hiscott, Overproduction of NFKB2 (lyt-10) and c-Rel: a mechanism for HTLV-I Tax-mediated trans-activation via the NF-kappa B signalling pathway, Oncogene 9 (1994) 841–852.
[14] T. Murakami, H. Hirai, T. Suzuki, J. Fujisawa, M. Yoshida, HTLV-1 Tax enhances NF-kappa B2 expression and binds to the products p52 and p100, but does not suppress the inhibitory function of p100, Virology 206 (1995) 1066–1074.
[15] L. Petropoulos, J. Hiscott, Association between HTLV-1 Tax and I kappa B alpha is dependent on the I kappa B alpha phosphorylation state, Virology 252 (1998) 189–199.
[16] Z. Chu, J. DiDonato, J. Hawiger, D. Ballard, The tax oncoprotein of human T-cell leukemia virus type 1 associates with and persistently activates IkappaB kinases containing IKKalpha and IKKbeta, J. Biol. Chem. 273 (1998) 15891–15894.
[17] R. Geleziunas, S. Ferrell, X. Lin, Y. Mu, E.J. Cunningham, M. Grant, M. Connelly, J. Hambor, K. Marcu, W. Greene, Human T-cell leukemia virus type 1 Tax induction of NF-kappaB involves activation of the IkappaB kinase alpha (IKKalpha) and IKKbeta cellular kinases, Mol. Cell. Biol. 18 (1998) 5157–5165.
[18] M. Uhlik, L. Good, G. Xiao, E.W. Harhaj, E. Zandi, M. Karin, S.C. Sun, NF-kappaB-inducing kinase and IkappaB kinase participate in human T-cell leukemia virus I Tax-mediated NF-kappaB activation, J. Biol. Chem. 273 (1998) 21132–21136.
[19] M. Yin, L. Christerson, Y. Yamamoto, Y. Kwak, S. Xu, F. Mercurio, M. Barbosa, M. Cobb, R. Gaynor, HTLV-I Tax protein binds to MEKK1 to stimulate IkappaB kinase activity and NF-kappaB activation, Cell 93 (1998) 875–884.
[20] A.M. O'Mahony, M. Montano, K. Van Beneden, L.F. Chen, W.C. Greene, Human T-cell lymphotropic virus type 1 tax induction of biologically Active NF-kappaB requires IkappaB kinase-1-mediated phosphorylation of RelA/p65, J. Biol. Chem. 279 (2004) 18137–18145.
[21] G. Xiao, M.E. Cvijic, A. Fong, E.W. Harhaj, M.T. Uhlik, M. Waterfield, S.C. Sun, Retroviral oncoprotein Tax induces processing of NF-kappaB2/p100 in T cells: evidence for the involvement of IKKalpha, EMBO J. 20 (2001) 6805–6815.

Available online at www.sciencedirect.com
ScienceDirect
Biochemical and Biophysical Research Communications 355 (2007) 937–943
BBRC
www.elsevier.com/locate/ybbrc

Tgat oncoprotein functions as a inhibitor of RECK by association of the unique C-terminal region

Tsuyoshi Mori, Ryozo Moriuchi *, Eiko Okazaki, Kenji Yamada, Shigeru Katamine

Department of Molecular Microbiology and Immunology, Nagasaki University Graduate School of Biomedical Sciences, 1-12-4 Sakamoto, Nagasaki 852-8523, Japan

Received 8 February 2007
Available online 20 February 2007

Abstract

We identified RECK, a membrane-anchored glycoprotein negatively regulating the activities of MMPs, as a molecule interacting with Tgat oncoprotein consisting of RhoGEF domain and the unique C-terminal 15 amino acids. The Tgat increased the invasive potential of NIH3T3 cells expressing endogenous mouse RECK and this effect was partially inhibited by the co-expression of human RECK. On the contrary, the expression of exogenous human RECK in HT1080 cell line lacking the endogenous RECK expression reduced its invasive activity, which was recovered by the Tgat co-expression. Moreover, a Tgat mutant lacking the C-terminal region lost the potential to compete the function of RECK in HT1080 cells. These findings indicate that Tgat is the functional inhibitor of RECK, and the activation of MMPs induced by Tgat is likely to enhance invasive activities of cancer cells expressing Tgat.

Keywords: Tgat; Rho-GEF; RECK; MMP; Cell invasion; HTLV-1; ATL

In the previous study, we identified a novel transforming gene, *Tgat*, *trio*-related transforming gene, from a cDNA library derived from fresh leukemia cells from a patient with adult T-cell leukemia (ATL) [1]. *Tgat* expression in NIH3T3 mouse fibroblast cell line resulted in a loss of contact inhibition and the cells acquired the potential of anchorage-independent growth (colony formation in a semi-solid media). Subcutaneous injection of the *Tgat*-transformed NIH3T3 cells produced tumors in athymic nude mice. Remarkably, NIH3T3 cells transformed by Tgat revealed the invasive activity in a Matrigel 12-times higher than that of untransformed cells.

Tgat is comprised of the Rho-specific guanine nucleotide exchange factor (RhoGEF) domain of a multifunctional protein, TRIO, and the unique C-terminal 15-amino acid sequence translated from the alternatively spliced *Trio* mRNA. Most RhoGEFs such as the Dbl family contain highly conserved structural motifs including a GEF domain highly homologous to Dbl, known as Dbl homology (DH) domain, and the adjacent pleckstrin homology (PH) domain [2]. The GEF domain interacts with the inactive GDP-bound GTPases and promotes the release of GDP and its subsequent exchange for GTP, whereas the PH domain regulates the subcellular localization of the protein as well as the GEF activity [3]. In contrast, Tgat does not contain the PH domain downstream of the RhoGEF domain but harbors the unique sequence at the C-terminus. Mutagenesis studies showed that either the deletion of the C-terminal 15 amino acids or replacement of them by the PH domain of TRIO abrogated the potential of Tgat to transform NIH3T3 and activate cell invasion [1]. On the other hand, a pharmacological inhibitor of Rho-associated kinase (ROCK) also inhibited transforming and invasion-enhancing activity of Tgat. These findings indicated that both C-terminal region and RhoGEF domain play important roles in the biological activities of Tgat.

Abbreviations: Tgat, trio related transforming gene in ATL tumor cells; RECK, reversion-inducing cysteine-rich protein with Kazal motifs; MMP, matrix metalloproteinase.

* Corresponding author. Fax: +81 95 849 7060.
E-mail address: ryozo@nagasaki-u.ac.jp (R. Moriuchi).

0006-291X/$ - see front matter © 2007 Elsevier Inc. All rights reserved.
doi:10.1016/j.bbrc.2007.02.051

In order to elucidate the molecular mechanisms of Tgat-induced malignant transformation, the present study was conducted to identify a molecule physically interacting with Tgat through the C-terminal unique sequence using the yeast two-hybrid screening. In this study, we have found that Tgat associated with RECK, tumor suppressor gene product, and inhibited the function of RECK.

Materials and methods

Plasmid constructs. The expression vectors for Tgat and its mutant, TgatPH2, were described previously [1]. The entire coding sequence of *Tgat* was subcloned into pCMV-Myc vector to obtain the plasmid pCMV-mycTgat. The DNA fragment encoding mouse RECK (mRECK) amino acids 160–641 was cloned into pCMV-HA vector. The entire coding sequence of human RECK (hRECK) amplified by RT-PCR (primers, 5′-GGAATTCGATATCCGGACATGGCGACCGTCCG-3′ and 5′-CGG GGTACCGTTAACTTCCGTGGGCAGTCAGTTAT-3′) was digested with restriction endonucleases, *Eco*RV and *Kpn*I, and subcloned into pBluescript II SK(−). The resulting was digested with restriction endonucleases, *Eco*RV and *Hpa*I, and subcloned into the retroviral vector pDON-AI to create the pDON- hRECK.

Yeast two-hybrid screening. A cDNA fragment encoding the C-terminal 15 amino acids of Tgat (TgatC) was cloned into the pGBKT7 vector downstream of the DNA binding domain of GAL4 to generate the pGBKT7-TgatC bait. This bait was used to screen a NIH3T3/Tgat cDNA library constructed using pGADT7 vector. Putative positive clones were retransformed to the yeast strain with pGBKT7-TgatC or a nonspecific bait, pGBKT7. After this step of false positive elimination, specific clones were subjected to DNA sequencing and subsequent BLAST search analyses.

Cell culture. NIH3T3 cells and their transformants were grown in DMEM containing 5% calf serum, penicillin, and streptomycin. 293T cells and 293 10A1 packaging cell lines were grown in DMEM containing 10% FBS, penicillin, and streptomycin. HT1080 cells and their transformants were grown in MEM containing 10% FBS, penicillin, and streptomycin. Transient transfections of 293T cells were performed by the calcium phosphate method. The NIH3T3/Tgat, NIH3T3/Tgat+hRECK, HT1080/hRECK, HT1080/Tgat, HT1080/hRECK+Tgat and HT1080/hRECK+TgatPH_2 stable cell lines were established by infecting with retroviruses carrying the corresponding cDNAs.

Immunoblotting (IB) and co-immunoprecipitation (Co-IP) assays. Whole-cell lysates were prepared by lysing the cells in NP40 lysis buffer (10 mM Tris–HCl, pH 7.4, 150 mM NaCl, 1% Nonidet P-40, 1 mM EDTA, 1 mM phenylmethylsulfonyl fluoride, and one-hundredth volume of a protease inhibitor mixture). Cell lysates were added total volume of 2× SDS sample buffer (125 mM Tris-HCl, pH 6.8, 4% SDS, 20% glycerol, 10% 2-mercaptoethanol) and denatured, and then separated by SDS-containing polyacrylamide gel electrophoresis (SDS–PAGE), electro-transferred onto a polyvinylidene difluoride membrane. Following blocking with 5% fat-free dry milk in Tris-buffered saline-containing Tween 20, the membrane was probed with primary antibodies specific to each protein. The membrane was further probed with HRP-conjugated goat anti-mouse or rabbit IgG to visualize bands. For Co-IP assays, 293T cells were transfected with Myc-tagged Tgat expression vector, alone or in combination with various types of RECK expression vectors. 2.5% of the lysate was used for immunoblots of total protein extracts, while 40% of the lysates were incubated with primary antibodies specific to each protein for 1 h at 4 °C, and with Protein G Sepharose for another 16 h at 4 °C. The sepharose beads were washed four times with NP-40 lysis buffer, and the bound proteins were eluted in 1× SDS sample buffer and subjected to SDS-PAGE and IB analyses.

Measurement of the transcript of mRECK. Total RNA was isolated from cells by using the Trizol reagent according to the manufacturer's instruction. To remove contaminating DNA, samples were digested with DNase I. cDNA was generated from 2 μg of total RNA with the TheromoScript RT-PCR System for First-Strand cDNA Synthesis by using Oligo(dT) primer. The cDNAs were quantified by real-time PCR by using the LightCycler instrument. The condition for PCR was 45 cycles of denaturation (95 °C/10 s), annealing (60 °C/15 s), extension (72 °C/7 s). Primers were 5′-CTCAGAGTTCCTGTGAGT-3′ (forward) and 5′-TGG AGTCAGCCTATGAGC-3′ (reverse) for mRECK. Probes were 5′-TG TGTCTGGAAGCTGAGGGCTCA-3′ (fluorescein) and 5′-TGAAAA GCCGCTACCTGCCATG-3′ (LC Red 640) for mRECK. Primers and probes for mouse GAPDH were purchased from Roche Applied Science. Data were analyzed with LightCycler data analysis software.

Matrigel invasion assay. The Matrigel invasion assay was carried out according to the manufacturer's instruction. A 0.5 ml aliquot of NIH3T3 cells suspension at 2×10^5 cells/ml in DMEM supplemented with 0.1% BSA and 0.0005% ascorbic acid or HT1080 cells suspension at 0.5×10^5 cells/ml in MEM supplemented with 0.1% BSA was seeded on the upper chamber of Matrigel-coated transwell filters (8 μm pore). The medium supplemented with 5% calf serum or 10% FBS was added to the lower chamber and incubated for 22 h. Non-invading cells that remained on the upper surface of the filter were removed, and the cells that appeared on the lower surface of the filter were fixed with 100% methanol, stained and counted under a microscope. Each assay was carried out in triplicate.

Gelatin zymography. 5×10^5 cells/0.5 ml of NIH3T3 cells or 2.5×10^4 cells/0.5 ml of HT1080 cells were seeded into 12-well culture dishes. After 12–16 h, cells were cultured in serum free medium containing 0.1% BSA for 24 h. The conditioned medium was collected and then mixed with SDS sample buffer without reducing agent and separated on 10% acrylamide

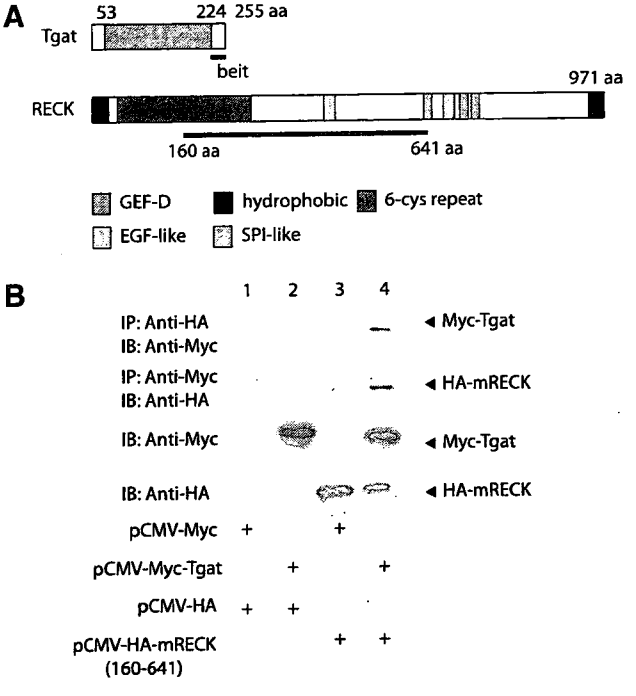

Fig. 1. Physical interaction between Tgat and RECK. (A) Structural configurations of the predicted Tgat and RECK protein. GEF-D, guanine nucleotide exchange factor domain; EGF, epidermal growth factor; SPI, serine protease inhibitor. The horizontal line below the RECK protein indicate the region that were obtained as interacting with COOH-terminal 15 amino acids residues of Tgat by using yeast two hybrid screening. (B) Direct interaction between Myc-tagged Tgat and HA-tagged mRECK. 293T cells were transfected with pCMV-mycTgat, pCMV-HAmRECK, and empty vectors with the indicated combinations. The lysates of transfected 293T cells were immunoprecipitated with anti-cmyc or anti-HA antibody. Total cell lysates and immunoprecipitates were separated by SDS/10% PAGE, and were immunoblotted with anti-cmyc, or with anti-HA antibody.

gels containing 0.1% gelatin. The gels were incubated in 2.5% Triton X-100 solution at room temperature with gentle agitation to remove SDS and then soaked in developing buffer (50 mM Tris–HCl, pH 7.5, 200 mM NaCl, 6 mM $CaCl_2$, 0.02% Brij 35) at 37 °C overnight. After the reaction, the gels were stained with Coomassie brilliant blue, and the gelatinolytic activities were visualized as clear bands against a blue background of stained gelatin. Quantitative analysis of gelatinase activities were measured by scanning the zymograms using Multi Gauge software Version 3.0 (Fujifilm).

Results

Identification of RECK as a Tgat-interacting molecule

We have previously shown that the C-terminal region of Tgat is essential to the transforming activity, colony-forming activity, and invasion activity in NIH3T3 and tumor formation in nude mice (1). To clarify the mechanism of transformation by Tgat, we made an attempt to identify molecules interacting with the C-terminal region of Tgat by yeast two-hybrid screening. We identified a cDNA encoding 482 amino acids from the cDNA library of NIH3T3 cells transformed by Tgat using the C-terminal 15 amino acids sequence of Tgat as a bait. As shown in Fig. 1A, the cDNA product was identical to mouse RECK (reversion-inducing cysteine-rich protein with Kazal motifs). To confirm the physical interaction of RECK with Tgat in mammalian cells, co-IP was performed using the NIH3T3 cells transformed by Tgat or 293T cells transfected with Tgat and mRECK expression plasmids. The interaction between Tgat and RECK could not be observed in the NIH3T3 cells transformed by Tgat because of the incapability of anti-mRECK antibody to detect the expression of endogenous mRECK. However, the transcripts of mRECK were found in the transformed NIH3T3 cells (Fig. S1). On the other hand, myc-tagged Tgat and HA-tagged mRECK formed a stable complex, which was readily precipitated from the cell lysates by the anti-HA and anti-Myc antibodies in the transfected 293T cells

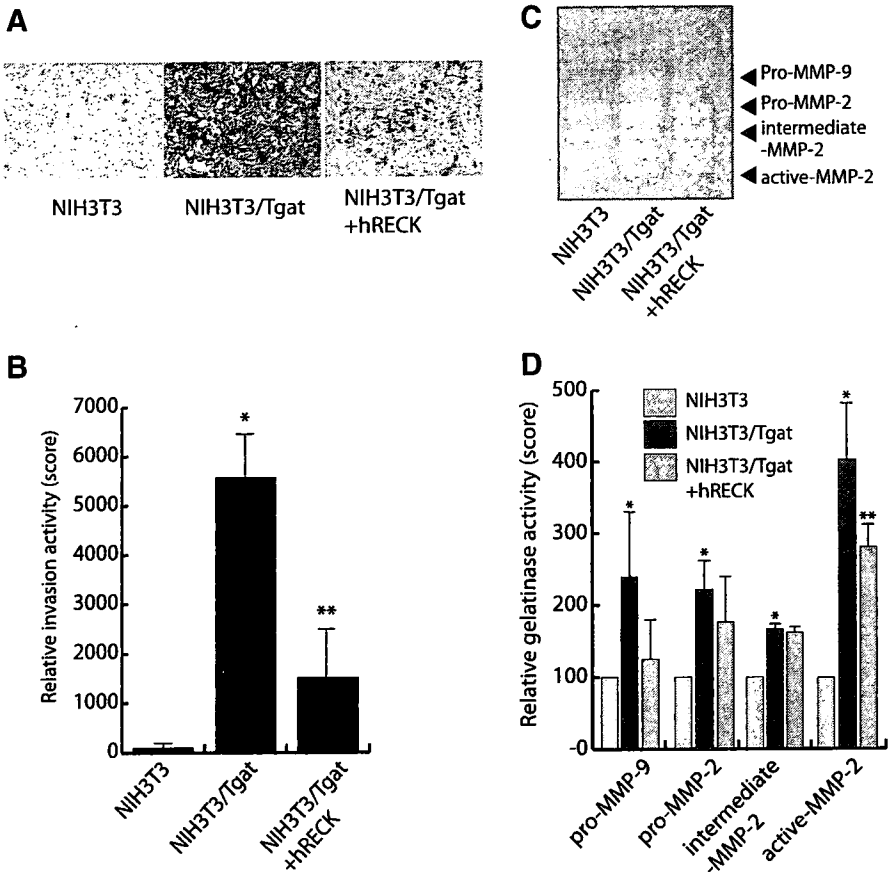

Fig. 2. Expression of Tgat enhances cell invasion level in NIH3T3 cell line. (A) Giemsa-stained migrated cells in Matrigel invasion assay. NIH3T3, untransfected NIH3T3 cells; NIH3T3/Tgat, those transfected with Tgat; NIH3T3/Tgat+hRECK, those co-transfected with Tgat and hRECK. (B) Relative invasion activities. The migrated cells were stained and then counted under light microscopy. Average migrated cell numbers of NIH3T3 is determined as score 100 and invasive activities of NIH3T3/Tgat and NIH3T3/Tgat+hRECK are expressed as relative scores. Columns, means of triplicate determinations; bars, SD. Data analyzed by one-way ANOVA ($P < 0.001$) was followed by Tukey–Kramer multiple comparison test. *NIH3T3 and NIH3T3/Tgat ($P < 0.01$); **NIH3T3/Tgat and NIH3T3/Tgat+RECK ($P < 0.01$). (C) Gelatin zymogram with the conditioned media from NIH3T3, NIH3T3/Tgat or NIH3T3/Tgat+hRECK cells. (D) Relative gelatinase activities. Averages of gelatinase activities in NIH3T3 mediums were determined as score 100. Columns, means of triplicate determinations; bars, SD. Data analyzed by one-way ANOVA Turkey–Kramer multiple comparison test. *NIH3T3 and NIH3T3/Tgat ($P < 0.01$); **NIH3T3/Tgat and NIH3T3/Tgat+RECK ($P < 0.01$).

(Fig. 1B). To examine whether Tgat interacts with full-length human RECK (hRECK), we isolated the cDNA encoding full-length 971 amino acids from human uterine cervix RNA by RT-PCR. Co-IP was performed using 293T cells transfected with hRECK and the Tgat expression plasmids. As shown in Fig. S2, hRECK also efficiently formed a complex with Tgat.

Tgat enhances cell invasion and inhibits RECK-dependent down-regulation of MMP activities in NIH3T3 cells

Since RECK was known to play a role in the cell motility by regulating the MMPs activities, we examined the effect of Tgat on the invasive activity of NIH3T3 fibroblast. Matrigel invasion assays revealed that Tgat potently increased the invasive activity of NIH3T3 (Fig. 2A and B). Gelatin zymography detected significant increase in the activities of active MMP-2 in the culture media of Tgat-expressing NIH3T3 whereas lesser increase of proMMP-9 activity was observed (Fig. 2C and D). Since untransfected NIH3T3 cells expressed a sufficient amount of mRECK mRNA (Fig. S1), Tgat was likely to interact with the endogenous mRECK and presumably competed its function. When hRECK was coexpressed in NIH3T3, the cell invasive capability and MMP-2 activation induced by Tgat were partially but significantly inhibited (Fig. 2D).

Tgat does not enhance cell invasion in HT1080 cells lacking RECK expression

To confirm the functional interaction between Tgat and RECK, we next used human fibrosarcoma cell line, HT1080, lacking the expression of endogenous RECK. In contrast to NIH3T3, the invasive activity of HT1080 in Matrigel containing 10% FBS was not changed by the expression of Tgat (Fig. 3A and B). Since the invasive activity of HT1080 itself is very high in the presence of 10% FBS, we re-examined the effect of Tgat in Matrigel with 1% FBS. As shown in Fig. 3, the level of invasive activity of HT1080 was reduced by 60% but Tgat again gave no significant effect. Judging from these findings, it is suggested that the invasive capability of Tgat may require the expression of RECK.

Function of RECK is inhibited by the expression of Tgat through its C-terminal region

To confirm the enhancement of invasive capability induced by Tgat in RECK-expressing HT1080, we established HT1080/hRECK, HT1080/hRECK+Tgat, and HT1080/hRECK+PH2 cell lines. The invasive activity of the HT1080/hRECK was reduced by 60%. When Tgat was co-expressed, the effect of hRECK almost completely abrogated (Fig. 4A). In other words, Tgat enhanced the invasive capability of HT1080/hRECK cells. On the contrary, a Tgat mutant lacking the unique 15 amino acids, the C-terminal region of Tgat was replaced by the PH

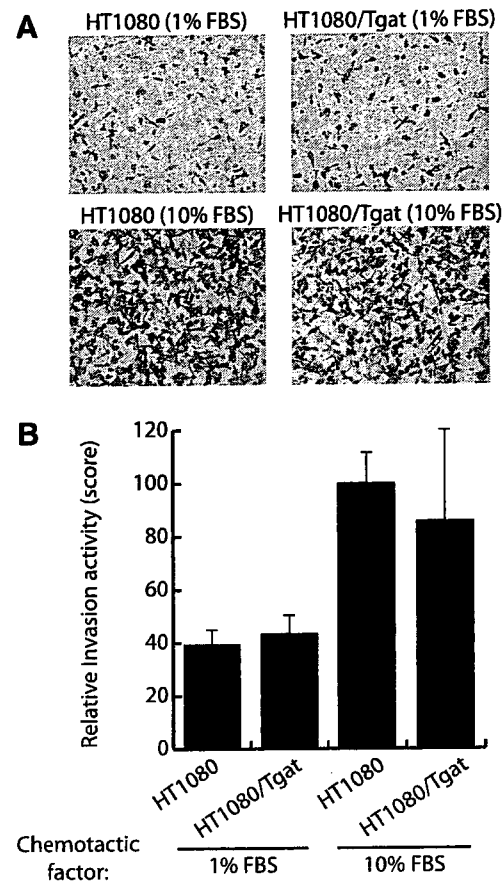

Fig. 3. Tgat fails to enhance cell invasion level of HT1080 cell line. (A) Giemsa-stained migrated cells in Matrigel invasion assay in the presence of 1% or 10% FBS. HT1080, untransfected HT1080 cells; HT1080/Tgat, those transfected with Tgat. (B) Relative invasion activities. The migrated cells were stained and then counted under light microscopy. Average migrated cell numbers of HT1080 in the presence of 10% FBS is determined as score 100 and invasive activities in the presence of 1% FBS and those of HT1080/Tgat are expressed as relative scores. Columns, means of triplicate determinations; bars, SD. Data analyzed by one-way ANOVA ($P < 0.05$) was followed by Tukey–Kramer multiple comparison test, however there is no significantly effect of Tgat in each groups of 1% FBS and 10% FBS treatments.

domain of TRIO, did not show the enhancement of invasion activity (HT1080/hRECK+PH2). Gelatin zymography also gave parallel results; levels of active MMP-2 and proMMP-9 in culture media of HT1080 were reduced by hRECK and Tgat abrogated the effect of hRECK, whereas not in HT1080/hRECK+PH2 cells (Fig. 4B).

Discussion

In this study, we have shown that Tgat is physically associated with RECK, a negative regulator of MMP-2 and MMP-9 activities, via the C-terminal unique sequence in the transfected NIH3T3 and HT1080 cells. The RECK gene was isolated as a transformation-suppressor gene using an expression cloning method designed to identify